Source-to-sink analysis in an active extensional setting: Holocene erosion and deposition in the Sperchios rift, central Greece

Sofia Pechlivanidou,* Patience A. Cowie,* Bjarte Hannisdal,* Alexander C. Whittaker,†
Robert L. Gawthorpe,* ⓘD Christos Pennos‡ and Ole S. Riiser*

*Department of Earth Science, University of Bergen, Bergen, Norway
†Department of Earth Science and Engineering, Royal School of Mines, Imperial College, London, UK
‡Department of Physical Geography, School of Geology, Aristotle University of Thessaloniki, Thessaloniki, Greece

ABSTRACT

We present a source–to–sink analysis to explain sediment supply variations and depositional patterns over the Holocene within an active rift setting. We integrate a range of modelling approaches and data types with field observations from the Sperchios rift basin, Central Greece that allow us to analyse and quantify (1) the size and characteristics of sediment source areas, (2) the dynamics of the sediment routing system from upstream fluvial processes to downstream deposition at the coastline, and (3) the depositional architecture and volumes of the Holocene basin fill. We demonstrate that the Sperchios rift comprises a 'closed' system over the Holocene and that erosional and depositional volumes are thus balanced. Furthermore, we evaluate key controls in the development of this source–to–sink system, including the role of pre–existing topography, bedrock erodibility and lateral variations in the rate of tectonic uplift/subsidence. We show that tectonic subsidence alone can explain the observed grain size fining along the rift axis resulting in the downstream transition from a braided channel to an extensive meander belt (>15 km long) that feeds the fine–grained Sperchios delta. Additionally, we quantify the ratios of sediment storage to bypass for the two main footwall–sourced alluvial fan systems and relate the fan characteristics to the pattern and rates of fault slip. Finally, we show that ≥40% of the sediment that builds the Sperchios delta is supplied by ≤22% of the entire source area and that this can be primarily attributed to a longer–term (~10^6 years) transient landscape response to fault segment linkage. Our multidisciplinary approach allows us to quantify the relative importance of multiple factors that control a complex source–to–sink system and thus improve our understanding of landscape evolution and stratigraphic development in active extensional tectonic settings.

INTRODUCTION

Temporal and spatial variations in sediment supply are widely recognized as key controls on stratigraphic architecture in sedimentary basins (Jordan & Flemings, 1991; Orton & Reading, 1993; Eliet & Gawthorpe, 1995; Paola, 2000; Forzoni *et al.*, 2014). Furthermore, the grain size of sediment released from mountain catchments is critical for facies development within basin-fills (Visher, 1969; Whittaker *et al.*, 2011; Allen *et al.*, 2015; Armitage *et al.*, 2015). At the same time the characteristics of the supply delivered to the basin margin are modulated by both autogenic and allogenic forcing conditions, such as the mechanisms that govern sediment transport and the spatial distribution of tectonic subsidence (Heller & Paola, 1992; Paola *et al.*, 1992; Fedele & Paola, 2007; Allen *et al.*, 2013).

During the last few decades, sediment delivery to depositional basins has increasingly been viewed within a source-to-sink framework, the aim being to dynamically link the surface processes within the different segments of an erosional – depositional system (e.g., Allen, 2008; Sømme *et al.*, 2009). The challenge has been to find natural systems for which sufficient constraints exist on each of the different segments of the entire system such that the key controls can be identified and evaluated. Simple source-to-sink systems that consist of an upland catchment and an adjacent fan are relatively well understood

Correspondence: Sofia Pechlivanidou, Department of Earth Science, University of Bergen, Allégaten, 41, N-5020 Bergen, Norway. E-mail: sofia.pechlivanidou@uib.no

(e.g., Allen & Densmore, 2000; Densmore *et al.*, 2007; Armitage *et al.*, 2011; Rohais *et al.*, 2012) and numerical models have been used to shed light on the geomorphic response of these systems to changes in both tectonic and climatic boundary conditions (e.g., Allen & Densmore, 2000; D'Arcy *et al.*, 2016). However, these models may not apply to larger and more complex erosional–depositional settings, such as that considered here, because they do not, for example, address multiple sites of sediment input and deposition within fault-controlled landscapes. On the other hand, workers such as Covault *et al.* (2010, 2011) and Sømme *et al.* (2011, 2013) reconstructed onshore - offshore sediment budgets for larger and more complicated natural examples but did not explicitly describe the dynamics of the sediment routing system. Matenco & Andriessen (2013) combined a wide range of surface and subsurface data to quantify sediment delivery to the Danube River Basin but the characteristics of the sediment supplied to the depositional system were not studied in detail.

Allen (2008) argued that to fully evaluate the surface processes from source to sink and to understand the system response to different forcing mechanisms it is important to consider how the characteristics of the sediment supply are transformed by the internal dynamics of the sediment routing system. Michael *et al.* (2013, 2014) and Hampson *et al.* (2014) have demonstrated this point explicitly by applying a mass-balance analysis to ancient sediment routing systems in the Spanish Pyrenees and Central US, respectively. These studies showed that the depositional extraction of gravel and sand was controlled by the spatial distribution of accommodation and, implicitly, by the characteristics of the sediment supply, even though the erosional source catchments are not preserved in these examples. In contrast, Whittaker *et al.* (2010) analysed Pleistocene to recent systems in the Central Apennines of Italy, providing quantitative data concerning sediment volumes and the down-system grain size fining for individual catchments that have experienced a transient response to tectonics. These data indicated that the volume, locus and grain size characteristics of sediment in the supply were clearly sensitive to the fault activity, but the authors had few constraints on the depositional sink. In summary, studies of well-constrained natural examples of complete source-to-sink systems that also consider the sediment routing system are rare.

In this study we seek to understand the controls on sediment delivery to a tectonically active setting in the Sperchios rift, Central Greece, during the Holocene (Fig. 1). We follow an integrated approach (Fig. 2) by analysing and quantifying (1) the size, spatial distribution and characteristics of sediment source areas, (2) the dynamics of the sediment routing system, and (3) the depositional architecture and volumes of the Holocene Sperchios basin fill. We implement a combination of methodologies that have only been seperately applied in previous source-to-sink studies and range from theoretical modelling of grain size distributions, numerical modelling of deltaic deposition, to methodologies that allow us to estimate catchment-averaged erosion rates and to assess the dynamics of the drainage network. We evaluate our modelling results against independent field observations from the different segments of the Sperchios erosional–depositional system. Using this multidisciplinary approach we are able to identify, quantify, and assess the relative importance of factors controlling the source-to-sink system in this active extensional setting and thereby develop a broader understanding of sediment supply variations and depositional patterns in rift basins.

BACKGROUND – THE SPERCHIOS RIFT

Tectonic setting

The Sperchios rift is the northernmost of the central Greece active rift basins that have formed due to crustal extension since the Early Pliocene (~5 Ma) (Leeder & Jackson, 1993; Kilias *et al.*, 2008). According to Goldsworthy *et al.* (2002), extension in the Sperchios rift began in the Middle Pliocene, approximately 3.6 Ma. It is characterized by an asymmetric half-graben geometry, approximately 100 km long, bounded along the south side by several major NW–SE striking, high-angle normal fault segments that dip towards the north (Fig. 1a). From west to east the three main faults, mentioned in this study, are the Sperchias, Kobotades and Thermopylae fault segments; collectively they are referred to as the Sperchios fault zone. Individual segments are typically 15–20 km long (Eliet & Gawthorpe, 1995) and display evidence of linkage along strike (Cowie *et al.*, 2008; Whittaker & Walker, 2015). Bedrock lithology is dominated by Paleogene flysch (sandstone and siltstone), outcropping mainly in the southwest and western parts of the study area, whereas Mesozoic ophiolite and limestone characterize the northern and southeastern margins of the rift respectively (Fig. 1a). Along the rift axis, alluvial and deltaic sediments have gradually filled the graben during the Plio-Quaternary.

Results from gravity modelling (Apostolopoulos, 2005) reveal several major rift depocenters that decrease in depth from east to west (Fig. 1b) and correspond to the major fault segments. Maximum basin depths reach ~2 km in the Maliakos gulf, estimated from the combined interpretation of resistivity and gravity measurements (Apostolopoulos, 2005). As the depth decreases towards the west, the width of the half-graben also decreases from ~15 km to < 5 km and as it narrows, basin asymmetry becomes more pronounced (Fig. 1b; see also Goldsworthy *et al.*, 2002). The Sperchias fault segment is the most
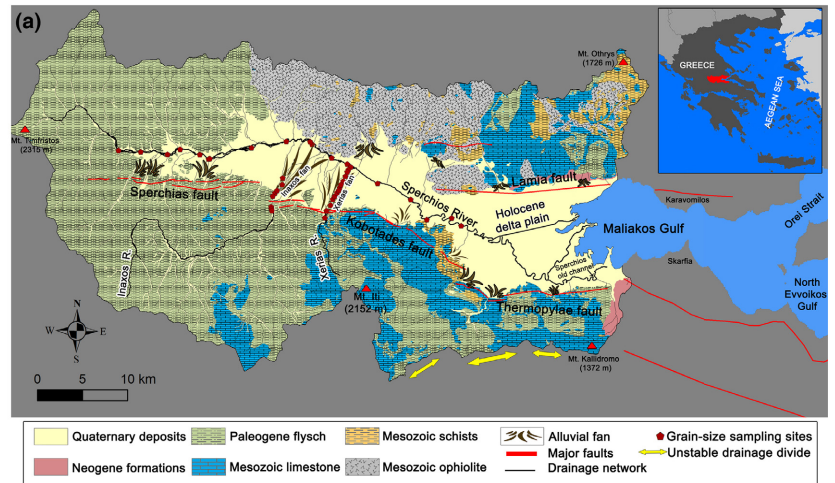
Fig. 1. (a) Geological map of the Sperchios rift basin. Yellow arrows refer to χ-analysis in supplementary Figure S3. (b) Map showing the basement relief (in meters) of the Sperchios rift derived from interpretation of resistivity and gravity measurements using a sediment density of 2200 kg m^{-3} (from Apostolopoulos, 2005). Basin volume (in m^3) of the four distinct depocenters is also shown. Black arrows indicate sediment input from the two large transverse alluvial fans, i.e., Inahos and Xerias (see Fig 6 b, c and 8).
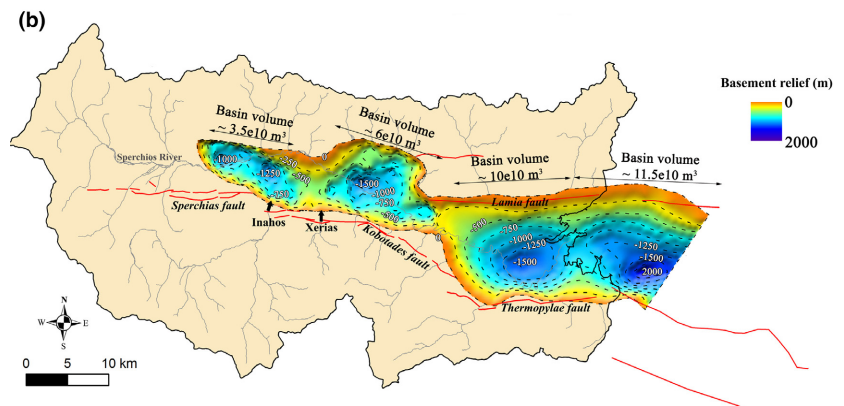
westerly segment and its western end defines the rift tip. In contrast, moving in an easterly direction, the fault off-sets gradually increase and the rift becomes less asymmetric as south-dipping (antithetic) faults develop along the northern margin of the graben (e.g., the Lamia fault, Fig. 3a).

Footwall relief is characterized by topographic highs (1500–2000 m) along the central portions of the major fault segments bounding the southern margin of the rift. In contrast, the hanging wall dip-slope, along the northern margin, is characterized by lower elevations (~600 m). Near the rift tip, to the west of the Kobotades fault segment in particular, pre-existing (i.e., pre-extension) topography dominates over the rift-related topography and the relief remains in excess of 2000 m well beyond the western tip of the Sperchias fault segment (e.g., Mt. Timfristos; Fig. 1a). Based on analysis of knick-point elevations along rivers draining across the Sperchias and Kobotades fault segments, Whittaker & Walker (2015) calculated that most of the rift-related relief in this area has formed since about 1.0–1.6 Ma when segment linkage occurred and fault slip rates increased so that currently, and thus during the Holocene, the rate of relative footwall uplift (i.e. relative to the

hanging wall basin fill) along the centre of the Kobotades segment is in the range 0.75–1.25 mm year^{-1}. Their preferred interpretation is that the lower estimate (0.75 mm year^{-1}) is more reasonable so that the total throw rate at the centre of the Kobotades segment is at least $2 \times 0.75 = 1.5$ mm year^{-1} (a minimum, based on uplift: subsidence ≤1). Both footwall relief and the hanging wall basin depths (Fig. 1b) decrease along the Sperchias segment, indicating a gradual reduction in extension rate in a westerly direction towards the rift tip (Goldsworthy et al., 2002). Our own modelling of the Sperchios delta (see *Results* below) places constraints on tectonic subsidence rates along the Thermopylae rift segment and confirms that the extension rate increases along strike towards the east.

Surface processes within the Sperchios rift basin

The Sperchios source-to-sink system is characterized by a major axial river, approximately 80 km long, which drains the upland catchments and flows from west to east, supplying sediment to the shallow marine gulf of Maliakos (~30 m water depth). The Maliakos Gulf is partially
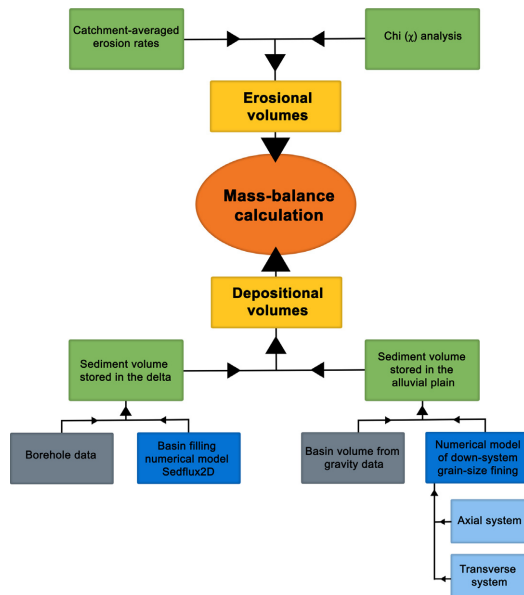
Fig. 2. Work flow diagram showing the methodology followed in this study to analyze the Sperchios source to sink system. The upper part of the diagram refers to the erosional system and depicts the methods used to quantify the spatial distribution and the characteristics of sediment source areas. The lower part of the diagram refers to the depositional system and depicts the methods used to quantify the dynamics of the sediment routing system and the volume of the Holocene Sperchios basin fill.

enclosed by two land spits (the Skarfia and Karavomilos spits, Fig. 1a) and little sediment is thought to by-pass into the north Evvoikos gulf further to the east (Eliet, 1995). Over the first ~ 50 km of downstream distance, the axial river migrates across a ~1 km wide braid plain (Fig. 1a). Subsequently, there is a transition to a meandering channel that continues to the shoreline and terminates in a bird's foot delta referred to as the Sperchios delta (Figs 1 and 3a). The transition from the braided to meandering fluvial domains occurs near the eastern end of the sub-basin bounded by the Kobotades fault segment. It coincides with the development of the south-dipping Lamia fault (Fig. 3a), thus a reduction in rift asymmetry, and an increasing extension rate towards the east (i.e., along the Thermopylae rift segment, Goldsworthy *et al.*, 2002). The position of the axial river along the rift is strongly influenced by the combination of footwall-sourced alluvial fans and tectonic subsidence along the Sperchios fault zone. For example, where the large, low angle (~0.7°) Inahos alluvial fan progrades into the basin, it clearly diverts the Sperchios River to the north (Fig. 1a). In contrast, along the Thermopylae fault segment the tectonic subsidence rate is sufficiently high that the location of the axial river was, until recently, close to the southern margin of the rift (i.e., prior to end of the

19th century when it became artificially controlled, see Sperchios 'old channel' in Fig. 1a). Along this segment, footwall-sourced alluvial fans have steep surface slopes (~2.5°) and do not prograde more than 1–2 km into the hanging wall.

Multi-proxy analysis and age constraints on deltaic sediments deposited along the Thermopylae segment of the rift (Fig. 1a) indicate that they developed as a transgressive to regressive succession during the Holocene (Fig. 3b; Pechlivanidou *et al.*, 2014) and consist mainly of fine-grained sediments (i.e., ~60% silt). These deposits are ~50 m thick and overlie alluvial plain deposits of Late Pleistocene - Early Holocene age (Pechlivanidou *et al.*, 2014). Within this succession ^{14}C determinations indicate a marine transgression rate of approximately 3.5 m year^{-1} for the Early Holocene. Maximum transgression pushed the shoreline 6–7 km to the west of its present location, inferred by the lateral extent of shallow marine deposits (i.e., FA3, see Fig. 3b). Progradation of the Sperchios delta since ~8000 cal. year B.P. and the current shoreline position indicate an average regression rate of ~1 m year^{-1} over this period.

METHODOLOGY

We begin our analysis with the deltaic depositional system, where we have particularly good constraints (c.f. Pechlivanidou *et al.*, 2014), and work progressively upstream by analysing the onshore fluvial system and ultimately quantifying the upland sediment sources. These different components are then brought together in a mass balance calculation for the whole erosional-depositional system in the Sperchios basin. The methods outlined below are summarized in a work flow diagram (see Fig. 2).

A minimum estimate of the volume of sediment preserved in the delta is obtained from boreholes that penetrate the transgressive - regressive succession of Holocene sediments (Fig. 3). We use these data to delineate the transgressive surface over which sediment was deposited during the Holocene and, by subtracting this 3D surface from the present-day topography based on a 5 m resolution DEM, we obtain an estimate of the volume preserved beneath the delta plain (Fig. 3c,d). However, to place constraints on the total (onshore and offshore) volume of the delta we implement the basin-filling numerical model Sedflux2D (Syvitski & Hutton, 2001; Hutton & Syvitski, 2008) to model the Holocene development of the delta. This model works by specifying an input sediment flux (volume, grain size, density and porosity) and outputs the thickness and the grain size variations of basin stratigraphy that can be compared with observations. The modelled profile is indicated in Fig. 3a and the input parameters are given in Table 1. Approximating the
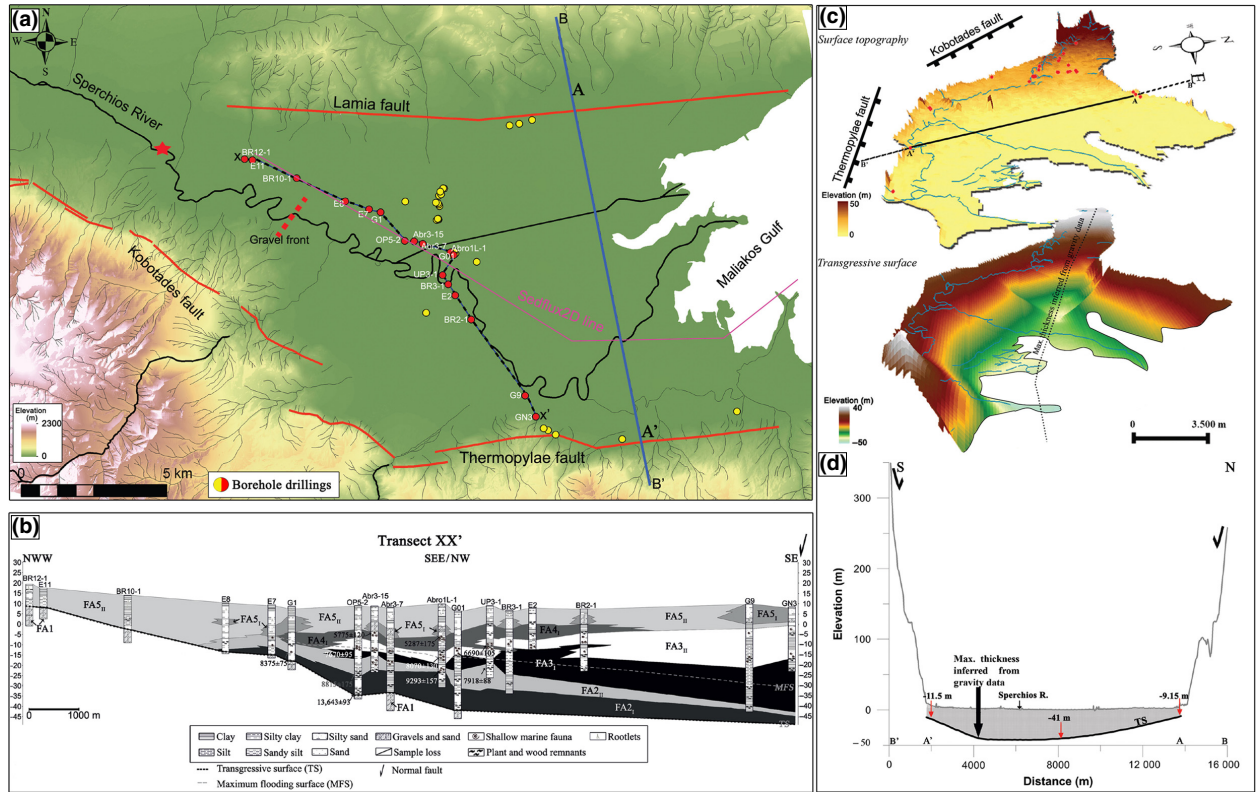
Fig. 3. (a) Map of the eastern part of the Sperchios rift (Thermopylae segment) showing the bird's foot delta. The transition of the Sperchios River from a braided to meandering channel is marked with a red star and the gravel front by a thick red dashed line. Red dots indicate the location of borehole drillings used to construct the Holocene stratigraphy of the delta along XX' transect, shown in Fig. 3b (from Pechlivanidou *et al.*, 2014). Yellow dots indicate the location of the additional borehole drillings used in this study to produce the 3D geometry of the transgressive surface (TS) shown in Fig. 3c. Blue solid line indicates transect BB' (see Fig. 3d). Line indicating Sedflux2D modelled profile is also shown (see Figs 4 and 5). (b) The stratigraphic model of the Holocene Sperchios delta after Pechlivanidou *et al.*, (2014). Facies associations are indicated; FA1: Fluvial, FA2I: Coastal plain, FA2II: Back–barrier lagoon, FA3I: Prodelta, FA3II: Delta front, FA4I: Open lagoon, FA5I: Channel fill, FA5II: Floodplain. Arrow shows the Thermopylae fault to the SE of the Sperchios rift; ^{14}C ages are in cal. yr B.P. (c) Digital elevation model (5 m resolution) of the meandering channel domain and the present delta plain (upper figure) and the 3D geometry of the Holocene TS (lower figure). Red circles at the upper figure indicate the borehole drillings used to construct the TS surface in 3D. Transects AA' and BB' indicate the profiles show in Fig. 3d. Black arrows indicate the Sperchios border fault zone. Maximum sediment thickness inferred from geophysical investigations is shown with a dashed line at the lower figure. (d) Cross section AA' showing the asymmetry of the Holocene TS surface in a N-S direction. The present topography is also shown along cross section BB'. Red arrows indicate the depth (in meters) of the TS at the northern, southern and central part of cross section AA'. The maximum thickness inferred from geophysical data is shown with a black arrow.

geometry of the delta using a 2D model is justified in this case by the fact that it is largely confined to build axially by the rift bounding faults (Fig. 3). We include Holocene sea level variations according to that proposed by Lambeck & Purcell (2005) for the Aegean Sea, which is dominated by a rapid marine transgression until ~6000 years B.P. Due to low wave activity in the Maliakos Gulf (Poulos *et al.*, 1997) we ignore erosion processes and sediment reworking by waves. The initial surface along which sediment is deposited in the model is our estimate of the shape of the bathymetry at ~10 000 years B.P. Spatial adjustments were made to the initial bathymetry, consistent with known rates of tectonic subsidence (Eliet &

Gawthorpe, 1995; Whittaker & Walker, 2015; see Table 1). We assume a mean valley width of 7 km to take into account the cross-sectional geometry of the rift. This allowed us to go from a two-dimensional line to a volume estimate. We validate the results by comparing the model output with the stratigraphic interpretation of Pechlivanidou *et al.* (2014) and thereby constrain the Holocene-averaged sediment load supplied to the delta.

The Holocene sediment volume stored in axial depocentres along the onshore part of the Sperchios rift may be estimated from available geophysical data (Fig. 1b) and knowledge of the age of the rift. However, this approach assumes average sedimentation rates apply

Table 1. Input parameters used to simulate Sperchios delta (Sedflux2D)

Model resolution	
Simulation time (year)	10 000
Time step (year)	10
Horizontal grid cell size (m)	100
Vertical grid cell size (m)	0.01
Mean basin width (m)	7000
Profile length (m)	25 000
Grain size	
Number of grain size classes	6
Grain size (μm)	350, 100, 40, 10, 5, 2
Grain density (kg m^{-3})	2650, 2625, 2600, 2550, 2500, 2450
Saturated density (kg m^{-3})	2000, 1950, 1900, 1850, 1800, 1750
Minimum porosity (-)	0.30, 0.20, 0.15, 0.1, 0.07, 0.05
Compaction coefficient (1 × 10^8)	3.6, 5, 7, 8, 10, 36
Tectonic subsidence (m year^{-1})	
From 0 to 8 km	0.0005
From 8 to 13 km	Linear increase from 0.0005 to 0.0015
From 13 to 25 km	0.0015

for the entire duration of rift basin development. Thus, to constrain better the Holocene depositional volumes, as well as to analyse the dynamics of the sediment routing system, we quantify the present-day grain size distributions for the axial river and two major transverse alluvial fans that supply sediment to the axial system (Inahos and Xerias fan, see Fig. 1 for location). We explore the relationships between sediment caliber, the amount of supplied sediment and accommodation creation along the Sperchios rift by implementing the grain size fining model of Fedele & Paola (2007), developed for stratigraphic use by Duller *et al.* (2010). This methodology is based on the concept that grain size distributions in gravel rivers are self-similar i.e., both the mean and standard deviation decay at a similar rate downstream, and explains reduction in grain sizes in fluvial systems as a function of sediment supply and tectonic subsidence via the processes of selective transport and deposition of sedimentary particles. The potential contribution to down-stream fining from abrasion is also considered. We estimate the coarse fraction (>1 mm) sediment caliber based on the Wolman point count technique using scaled grain size photos (Attal & Lavé, 2006; Whittaker *et al.*, 2010, 2011) at 40 localities (see red dots on Fig. 1a). We measure the intermediate axis of ~11500 clasts and we obtain cumulative frequency distributions from which estimates of the median grain size value D_{50} were derived as well as the mean and the standard deviation values of the grain size distributions (following Whittaker *et al.*, 2011).

Constraints on relative tectonic uplift rates where rivers cross active normal faults (e.g., Whittaker & Walker, 2015) enable us to make a first order estimate of the volume of sediment released from upland areas. We assume that the rate of relative tectonic uplift, U, is balanced by the rate of erosion E, at the point where the Inahos River crosses the Kobotades fault (see Fig. 1 for location). Based on our field measurements of local channel slope, S, and high flow channel width, W, we calibrate the erodibility coefficient K, in the stream-power erosion model:

$$E = K \frac{A^m}{W} S^n \tag{1}$$

where m and n are positive, empirical coefficients (Whipple & Tucker, 1999), A is the upstream drainage area (as a proxy for water discharge Q) and K is a parameter that subsumes factors such as substrate erodibility and climate. We use our estimate of K to calculate the catchment-averaged erosion rates and thus the long-term sediment supply from catchments with the same bedrock lithology (in this case the Paleogene flysch; Fig. 1a). The advantage of this simple approach is that it does not require that the landscape is in steady state. The empirical channel width model (Finnegan *et al.*, 2005) best describes our measurements of channel width so that:

$$E = KA^{5/8} S^{19/16} \tag{2}$$

This relationship accounts for dynamic channel adjustment and allows variations both in channel width, W, and channel slope, S, to control incision rates in tectonically active areas (Whittaker *et al.*, 2007; Attal *et al.*, 2008, 2011). A and S were readily extracted from a high-resolution DEM (5 m) (copyright © 2012, Hellenic Cadastre). We applied Eqn (2) to every pixel along the stream network using all channels down to first order and interpolated the obtained erosion rates across the whole catchment area.

Finally, we use the statistical tool of Mudd *et al.* (2014), based on the integral method of channel profile analysis, to assess spatial variations in erosion rates. The integral of drainage area over flow distance produces the transformed coordinate known as χ, which has dimensions of length (Perron & Royden, 2013; Royden & Perron, 2013). We map the slope of transformed channel profiles ($M\chi$) across individual catchments. In addition, we compare values of χ on opposite sites of the main Sperchios drainage divide for all catchments with a base-level at the coast, following the approach of Willett *et al.* (2014), in order to assess whether the size and extent of upland source areas may have changed as a result of drainage reorganization.
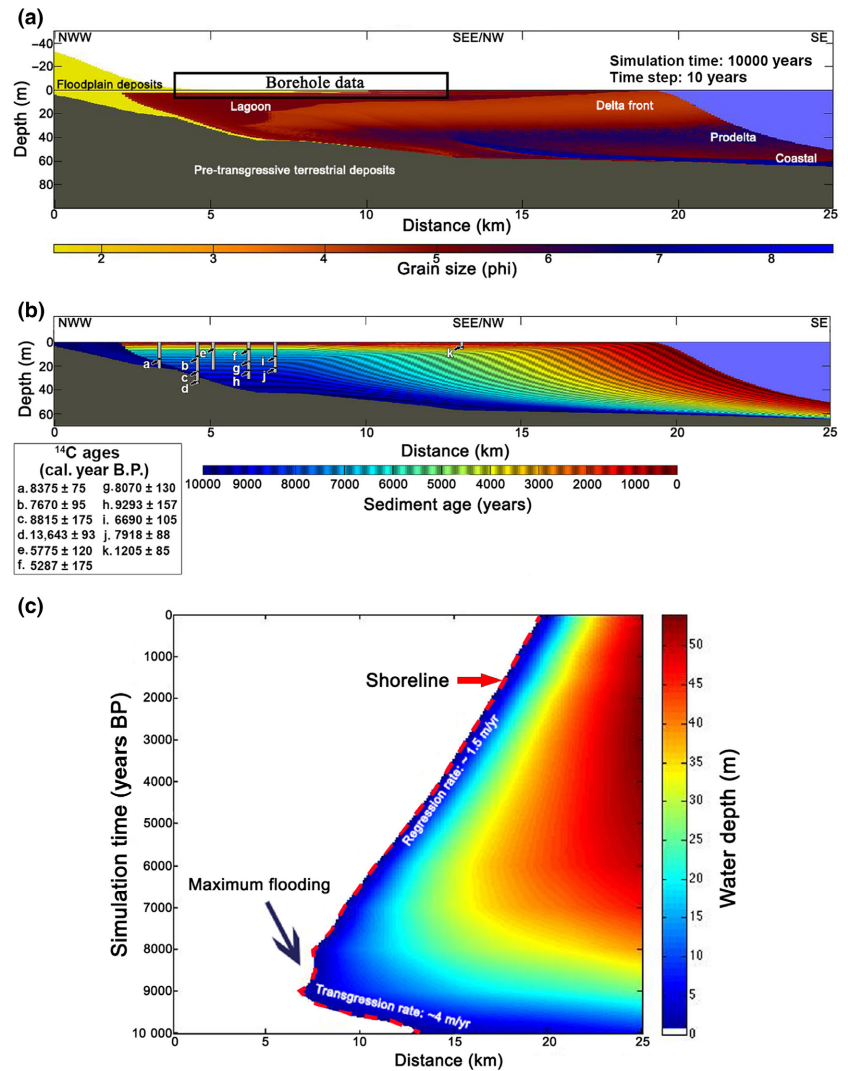
Fig. 4. Sedflux2D prediction of the Sperchios delta evolution during the Holocene. Simulations run along the profile shown in Fig. 3a using a Qs of 1.0 x 10^6 m^3 year^{-1}. (a) Cross section of grain size (in phi units). Yellow colors at the base and the top of the deltaic succession represent sandy fluvial sediments. Red to blue colors represent silty to clayey shallow marine deposits that consist the transgressive - regressive Holocene wedge that overlies the pre-transgressive deposits shown with grey color. The area where there are borehole data is also indicated. (b) Cross section of sediment age (in years). Warmer colors indicate younger sediments and cooler colors indicate older sediments. Age constraints (after Pechlivanidou *et al.*, 2014) from borehole drilling are shown. (c) Chronostratigraphic plot showing temporal and spatial water depth variations. Red dashed line indicates the shoreline position through time and black arrow shows the maximum flooding. Rates of transgression and regression (in m/yr) are also indicated. Full description of the Sedflux2D modeling is given in Pechlivanidou, 2012.

RESULTS

Volume of sediment preserved in the Sperchios delta

The relief of the present-day Sperchios delta plain, the meandering fluvial domain, and the 3D geometry of the transgressive surface (TS) over which sediment was deposited during the Holocene are shown in Fig. 3c,d. The maximum depth of the TS (~50 m below m.s.l.) occurs close to the Thermopylae fault segment, consistent with geophysical constraints (see dotted line in Fig. 3c) and the asymmetric graben geometry. The difference between the topographic surface and the TS surface (Fig. 3c) indicates a minimum estimate of the Holocene delta volume of ~0.5 × 10^{10} m^3 as it only accounts for the volume preserved in the delta plain.

To account for the amount of sediment that lies in the subaqueous part of the delta, we use Sedflux2D to model the Holocene delta development (see Figs 4 and 5). The

value of sediment load (q$_s$) that we use in the initial model run (i.e., 1.0 × 10^6 m^3 year^{-1}, Fig. 4) is greater than the estimate from the volume calculation for the delta plain only as this is an under-estimate. We then test this assumption below (see Fig. 5). The cross-section of predicted grain size variation (Fig. 4a) depicts the transgressive to regressive geometry of the modeled Sperchios deltaic succession in a NW to SE direction. Facies associations (FA) recognized from borehole data (Fig. 3b) are comparable with model predictions in terms of the overall geometry, grain size and thickness. Medium to very fine silt and clay sediments (5–8 phi, i.e., 31–3.9 μm) overlie the pre-transgressive terrestrial deposits (FA1, in Fig. 3b) and reflect the coastal and distal prodelta transgressive sediments observed in the stratigraphy of the Sperchios delta (FA2 and FA3$_I$, in Fig. 3b). The total transgressive succession has a maximum thickness of approximately 25 m, which also matches field observations. Fine sand to coarse silt deposits (3–5 phi, i.e., 125–31 μm) overlie the
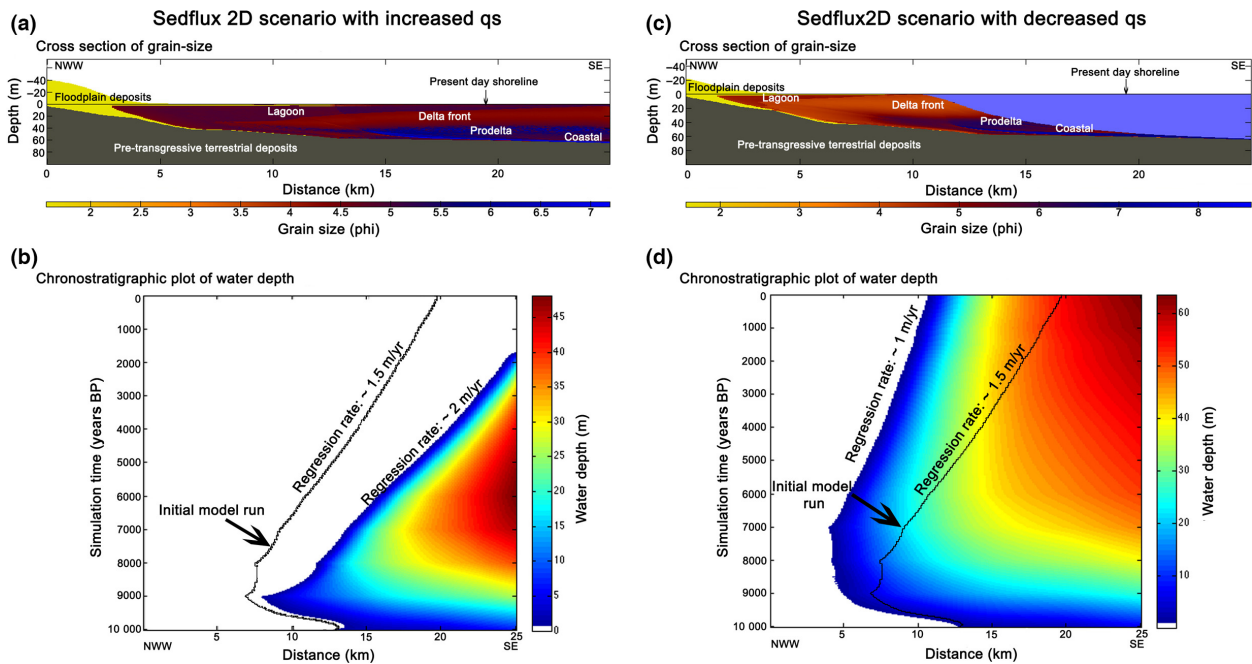
Fig. 5. Sedflux2D sensitivity experiments that show the effect of variable sediment load (qs) to the predicted stratigraphy and the water depth variations with time. Sedflux2D scenarios using qs value of 2×10^6 m^3 year^{-1} are shown in (a) and (b) and model scenarios with qs value of 0.5×10^6 m^3 year^{-1} are show in (c) and (d). The present day shoreline position is marked in the cross sections of grain size for comparison with the results of the sensitivity experiments. Black lines in the chronostratigraphic plots of water depth (b) and (d) indicate the shoreline position through time derived from the initial model run. Note difference in regression rates between the initial model run and the sensitivity experiments due to sediment supply variation.

transgressive sediments (Fig. 4a). These deposits depict a maximum thickness of ~30 m and comprise an overall upward shallowing lithological succession that reflects the highstand deposition (i.e., delta front and lagoonal deposits) observed in the published stratigraphic data (e.g., FA3$_{II}$ and FA4, in Fig 3b). The Holocene delta plain development is characterized by coarse to medium sand (2 phi, i.e., 250 μm) in Sedflux2D simulation. The model output does not fully reproduce the geometry and thickness of the floodplain deposits (see FA5, in Fig. 3b), but this does not significantly affect our volume estimate.

The cross-section of sediment age (Fig. 4b) shows the modelled temporal evolution of the Sperchios deltaic succession and the predicted distribution of sediment age. Age constraints derived from dating of shallow marine fossils collected from borehole samples (Pechlivanidou et al., 2014) indicate a succession from early to late Holocene and match the model predictions within a range of ± 700 years. The position of the shoreline through time, shown by the chronostratigraphic plot (Fig. 4c), enables us to estimate shoreline migration rates and verify that they are also consistent with the rates indicated by the field data. In addition, the timing and position of the maximum flooding (i.e., 8000 years B.P. at a distance of ~6–7 km further west) agrees with the observed stratigraphy

of the Holocene deltaic succession (see Fig. 3b). Based on these model results, calibrated using grain size analysis of core samples (see Table 1), we estimate a volumetric supply of 1.0×10^6 m^3 year^{-1} of sediment has been delivered and stored in the Holocene delta plain and subaqueous realm. In addition, our Sedflux modelling of the delta enables us to place tighter constraints on tectonic subsidence rates in this portion of the rift and indicate that the rate increases across strike from ~0.5 mm year^{-1}, close to the Lamia fault on the northern margin, to ~1.5 mm year^{-1} in the proximal hanging wall to the Thermopylae fault (Table 1).

To assess this result we conduct sensitivity tests (Fig. 5) where we vary the initial value of sediment load (q$_s$) over a range of ± 50% (q$_s$ = 2×10^6 m^3 year^{-1} (Fig. 5a,b) and q$_s$ = 0.5×10^6 m^3 year^{-1} (Fig. 5c,d)). All other input parameters are kept constant. Neither scenario matches the observations. In the case where we increased the value of q$_s$, the facies associations are shifted basin-wards and the position of the shoreline at the end of the simulation is located further east from its present location, thus implying a greater regression rate, inconsistent with the field data (Pechlivanidou et al., 2014). Moreover, regression commences almost 1000 years earlier than the field data suggest. In contrast, in the low sediment supply

Fig. 6. Down-system variations of the median grain size (D50 in mm) for the axial river (a) and the two transverse fans (b) and (c). Inset shows the location of the grain size measurements (see also Fig. 1a). Black arrows indicate the profiles used to model down-system grain sizes shown in Figs 7 and 8, for the axial and the transverse systems, respectively. Error bars on each measurement represent D40 and D60 values. Note the locally higher grain size values along the axial river that indicate lateral sediment input from the Inahos and Xerias fans.
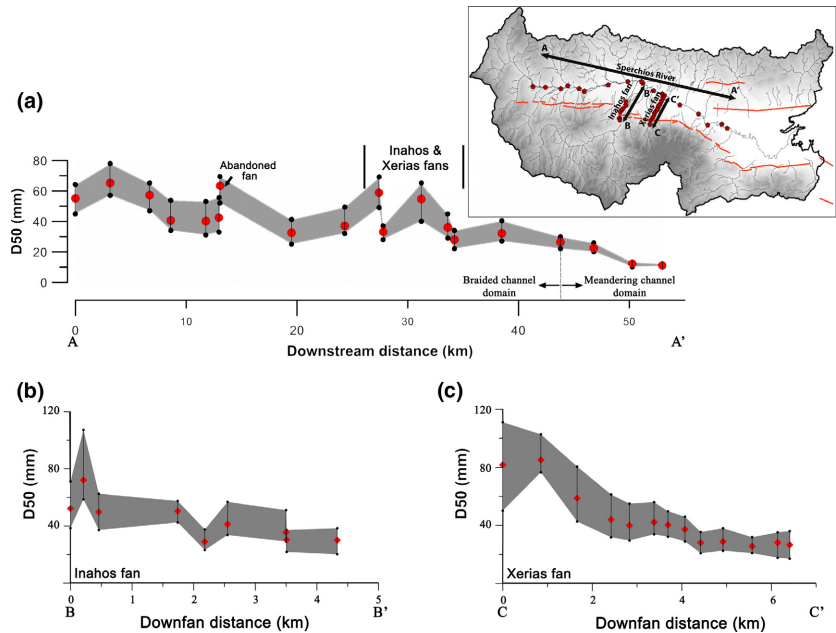
scenario (Fig. 5c,d), the position of the shoreline is ~8 km westwards from its present location and regression commences at a lower rate almost 1000 years later (i.e., from 7000 years B.P.) than in our initial model run and the field data suggest. We therefore conclude that our estimated volumetric supply rate of 1.0×10^6 m^3 $year^{-1}$ of sediment to the delta is reasonable.

Volume of sediment stored in the alluvial plain – geophysical constraints

Using geophysical constraints that indicate hanging wall stratigraphic fill thicknesses (see basement relief map, Fig. 1b) combined with information about the age of the rift (Goldsworthy *et al.*, 2002) we can estimate approximate volumetric sedimentation rates along the rift where it is occupied by the Sperchios River. This calculation assumes that sediment rates have remained constant over time and thus provides only a first order constraint. For example, if the rift basins in this area formed ~3.6 Ma (Goldsworthy *et al.*, 2002) then the average volumetric sedimentation rate, for the hanging wall sub-basins adjacent to the Sperchias and Kobotades faults segments combined, is $(9.5 \times 10^{10})/(3.6 \times 10^6)$ m^3 $year^{-1} = 2.6$ 10^4 m^3 $year^{-1}$ (for basin volumes see Fig. 1b). A maximum estimate of the rate is obtained if we assume that most of the offset on the basin bounding faults has accumulated since ~1.6 Ma (Whittaker & Walker, 2015), i.e., $(9.5 \times 10^{10})/(1.6 \times 10^6)$ m^3 $year^{-1} = 5.9 \times 10^4$ m^3 $year^{-1}$. These rates imply that the volume of material deposited over the Holocene (10 kyrs) in this part of the rift is in the range 2.6–5.9×10^8 m^3. Note that these volume estimates are nearly 2 orders of magnitude lower than those inferred for the Sperchios delta, consistent

with the smaller size of the hanging wall basins and lower throw rates along the Sperchias and Kobotades fault segments (Fig. 1b).

Volume of sediment stored in the alluvial plain - rates of downstream fining

An alternative way to quantify Holocene depositional volumes, more relevant to the recent history of depositional processes operating within the rift is to use the grain size fining model of Fedele & Paola (2007) (see Methodology). We use this model to obtain an estimate of the initial volumes (Q_{so}) of the coarse sediment fraction supplied to the axial river and to the two largest transverse alluvial fans (Fig. 1a) using published constraints on rates of tectonic subsidence $\sigma(\times)$ (e.g., Whittaker & Walker, 2015; see Figs 7b and 8c,d) plus our measurements of down-system grain size variations (Fig. 6). This approach not only provides an estimate of the total volume of gravel deposited along the rift axis but also provides additional constraints on the spatial distribution of deposition and thus the dynamics of the sediment routing system that supplies the Sperchios delta.

The grain size distributions of active gravel bars observed along the braided domain of the axial Sperchios River reveal fining downstream (Fig. 6a). The mean D_{50}, at the western tip of the rift is 57 ± 4.75 mm. Over the first ~30 km of downstream distance the mean grain size shows no systematic variation but at distances > 30 km downstream, in the hanging wall to the Kobotades fault, there is a pronounced decrease towards the east (Fig. 6a). The gravel front is located at a downstream distance of ~53 km, approximately coinciding with where the channel changes from a braided to a meandering morphology.

Both Inahos and Xerias alluvial fans also fine down-system from the fan apex (Fig. 6b,c, respectively) particularly over the first few kilometers of downstream distance.

According to the theory of Fedele & Paola (2007), grain size distributions in gravel rivers are self-similar with a constant value for the coefficient of variation, C_v. The grain size distributions of all our samples approximately match the theoretical prediction, justifying the use of the selective deposition theory to model our grain size data. In the supplementary file, the data used to calculate C_v as well as the similarity variable (ξ) are presented. Along the braided portion of the axial Sperchios River we find that $C_v = 0.64 \pm 0.1$, whereas the Inahos and Xerias alluvial fans are characterized by $C_v \sim 0.85$–0.88.

Grain size modelling - Axial Sperchios river

Figure 7 presents the grain size fining model results for the axial Sperchios River. For simplicity, we assume that tectonic subsidence $\sigma_{(\chi)}$ increases linearly from west to east along the rift axis, from ~0 to 1 mm year^{-1} (see Fig. 7b) based on published constraints on fault throw rates along the Sperchias and Kobotades fault segments (Whittaker & Walker, 2015) and the gradual increase in extension rate with distance along the rift from the tip (see *Background – Tectonic setting*; Goldsworthy *et al.*, 2002). Using a non-linear increase (e.g., Cowie & Shipton, 1998) does not significantly change our results (see, for comparison, a stepped increase Fig. S2).

The grain size fining model is based on a 2D calculation and thus we multiply the result by the active fluvial valley width to obtain the volumetric sediment supply in m^3 year^{-1}. We use the initial median grain size value that we obtained from our grain size data (i.e., $D_{50} = 57 \pm 4.75$ mm; Fig. 6a). The dimensionless parameter F_{qs} (Fig. 7) is the ratio of sediment supply (Q_s) to accommodation creation due to tectonic subsidence ($\sigma_{(\chi)}$). When $F_{qs} = 1$ the system is completely filled with coarse sediment (i.e., gravels) at the rate that accommodation is generated. Values of $F_{qs} > 1$ imply an overfilled system and values of $F_{qs} < 1$ imply that the system is underfilled (Duller *et al.*, 2010).

All of the model curves shown in Fig. 7 have a convex-up shape and the main difference between these curves is the predicted position of the gravel front. The measured grain size data (black dots) and the position of the gravel front are best described by $F_{qs} \approx 1$ (see red line in Fig. 7a) although there is some scatter that can be attributed to transverse sediment input. Even if the initial grain size is lower (e.g., 45 mm), $F_{qs} \approx 1$ describes well the downstream variation. Specifically, the linear increase in tectonic subsidence rate along strike assumed here (Fig. 7b) predicts that grain size varies little over the first ~30 km of downstream distance and then decreases rapidly close to the gravel
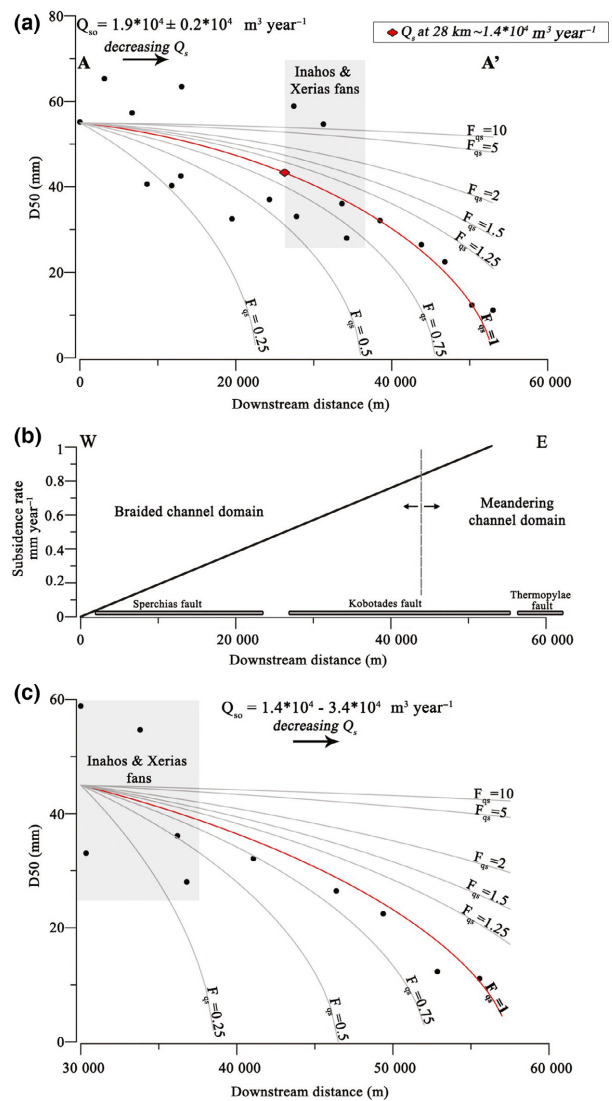

Fig. 7. (a) Grain size fining model results downstream along the axial river (AA', see Fig. 6). Black dots represent measured grain sizes and solid lines represent predicted grain size distributions for different values of the dimensionless parameter F_{qs}. The curve for $F_{qs} = 1$ and with the gravel front set at 53 km downstream is shown with a red solid line. The initial volume of the gravel fraction (Q_{so}) supplied to the axial system is also shown. Note that the amount of gravel decreases downstream due to mass extracted from the system. Grey box indicates the area of lateral sediment input from the Inahos and Xerias fans. (b) Spatial distribution of tectonic subsidence $\sigma_{(\chi)}$ along the Sperchios rift used to run the grain size fining model. Vertical dashed line marks the transition of the axial river from a braided to a meandering channel. (c) Grain size fining model results downstream the point where the Inahos River joins the axial river for different values of the dimensionless parameter F_{qs}.

front, consistent with the overall pattern of measured grain sizes (Fig. 7a). In contrast, a spatially uniform subsidence rate of 0.5 mm year^{-1} would predict gradual
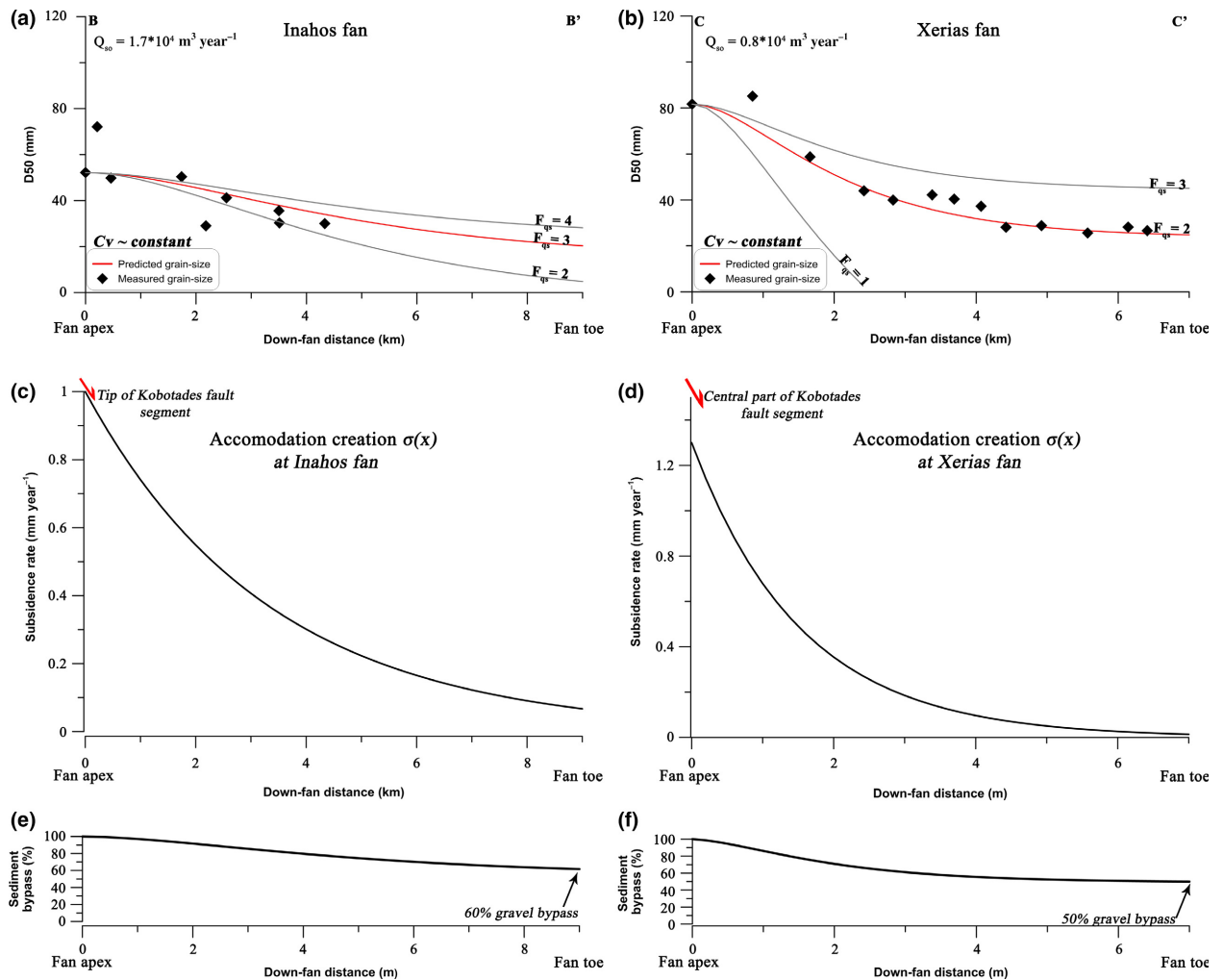
Fig. 8. Grain size fining model results for the Inahos fan (a) and Xerias fan (b) (BB' and CC', see Fig. 6). Preferred model predictions are shown with red solid lines. The initial gravel supply (Q_{so}) and the dimensionless parameter F_{qs} that fit the measured grain size data on both fans are also shown. Model runs performed using an exponential decrease in subsidence rate from the apex to the toe of the Inahos and Xerias fans, which is shown in (c) and (d), respectively. Red arrow indicates the Kobotades fault. (e) and (f) show the percentage of gravel bypasss (%) down-fan Inahos and Xerias, respectively. Note the percentage of sediment bypass to the axial river by the end of each system length (i.e., at the fan toes).

fining over the entire downstream distance and a less abrupt gravel front (Fig. S2).

We also considered abrasion as an alternative potential mechanism for the downstream variation in grain size, using the model of Attal & Lavé, 2006 (see Fig. S2). However, a mass loss per kilometer of 4–10% would be required to explain the observed amount of fining, which is high compared to laboratory estimates of abrasion rate (e.g. Attal & Lavé, 2009). Moreover, the abrasion model predicts a concave-up shape to the grain size trend and thus is inconsistent with what we observe (compare Figs 7 and S2). We cannot exclude abrasion as a contributing factor to grain size reduction but the independently-constrained west-to-east increase in subsidence rate (see *Background*) is able to account for the main

features of the fining trend along the axial river. By ignoring abrasion we may be underestimating the amount of gravel supplied by upstream source areas so our results are minimum estimates (see *Summary and Discussion*).

The $F_{qs} = 1$ curve implies that the basin is filled at exactly the rate accommodation is created and equates to a total gravel supply of $Q_{so} = 1.9 \times 10^4 \pm 0.2 \times 10^4$ m³ year⁻¹. Here we assumed an active fluvial valley width of 2.0 ± 0.2 km and that the subsidence rate in the centre of the hanging wall basin is half the maximum rate along the southern margin of the rift. This gravel volume is slightly lower but of similar order of magnitude to the independently derived geophysical estimate (i.e., 2.6–5.9×10^4 m³ year⁻¹; see above), which increases our level of confidence in this result. In this interpretation,

gravel is progressively extracted into stratigraphy until the gravel in the system is exhausted and the transition to the meandering channel occurs (Fig. 3a). It explains both the shape of the fining trend in the down-stream direction and why only the finer material (sand, silt and clay) reaches the delta plain to form the fine-grained Sperchios deltaic succession.

The curve $F_{qs} = 1$ (Fig. 7a) also predicts that, where the axial river is joined by the transverse system of Inahos, i.e., at ~28 km downstream (Figs 1a and 7a), only 25–30% of the gravel (~5 × 10^3 m^3 $year^{-1}$) derived from upstream has been extracted into the stratigraphy along the hanging wall to the Sperchias fault segment. The scatter in the grain size data makes it difficult to constrain the percentages precisely but most of the gravel (>70%; ~1.4 × 10^4 m^3 $year^{-1}$) is deposited along the basin bounded by the Kobotades fault segment. In order to investigate this conclusion further, and to test the sensitivity to valley width, we apply the grain size fining model from the point where the Inahos River joins the Sperchios River (Figs 1 and 7a,c). We use the mean measured grain size (i.e., 45 mm) observed near the toe of the Inahos fan and assume a linear increase in subsidence rate from 0.5 to 1 mm $year^{-1}$ along this section of the rift axis. This model (Fig. 7c) again shows a good fit between measured and predicted grain size data for $F_{qs} = 1$ with the observed location of the gravel front, and furthermore implies a volume of coarse sediment extracted into stratigraphy of 1.4 × 10^4–3.4 × 10^4 m^3 $year^{-1}$. This reflects a range of estimates of the active fluvial valley width along this section of the rift (2.0–5.0 km); the higher value therefore represents an upper estimate of the gravel extracted along the Kobotades fault segment.

Grain size modelling - Transverse alluvial fans

In order to account for the gravel trapped in the transverse alluvial fans that feed into the axial river (see Fig. 1), we again apply the mass extraction modelling methodology. The down-system widening of the fans is taken into account in these calculations (D'Arcy *et al.*, 2016). The results of the model are shown in Fig. 8a,b for the Inahos and Xerias fans, respectively. We assume that where the Inahos fan develops, in the zone of linkage between the Sperchias and Kobotades fault segments, the maximum subsidence rate along the fault is 1 mm $year^{-1}$, whereas the rate along the central part of the Kobotades fault segment where the Xerias fan develops is 1.25 mm $year^{-1}$ (see Fig. 8c,d respectively). These rates are consistent with the upper estimates inferred by Whittaker & Walker (2015) and take into account the different structural positions of these two fans plus the fact that in general hanging wall subsidence along extensional faults is greater than footwall uplift (Armijo *et al.*, 1996). We use an exponential decay function to describe the spatial distribution of proximal

hanging wall subsidence with distance from a normal fault (Allen *et al.*, 2015). The subsidence rate approaches zero at the toe of both fans to allow for the fact that accommodation at the fan toes is filled by the axial fluvial system. The median grain size value measured at the apex of the fans is used in the grain size fining model (i.e., $D_{50} = 52$ mm for Inahos fan and $D_{50} = 81.5$ mm for Xerias fan).

The exponential decay function successfully predicts the observed rapid fining over the first few km of down-stream distance (Fig. 8a,b). The volumes of sediment supplied to these fans (Q_{so}), inferred from the fits shown in Fig. 8a,b, are ~1.7 × 10^4 m^3 $year^{-1}$ for Inahos fan and ~0.8 × 10^4 m^3 $year^{-1}$ for Xerias fan. The predicted grain size distribution for both fans matches the measured field data for values of F_{qs} >1 ($F_{qs} = 3$, for Inahos and $F_{qs} = 2$, for Xerias), indicating that they are overfilled and that roughly 60% of the sediment released from the Inahos catchment bypasses the fan and enters the axial Sperchios River (Fig. 8e) and ~50% of sediment flux bypasses Xerias fan (Fig. 8f).

The lateral sediment input to the axial river from these two sources is reflected in locally higher grain size values (e.g., at 27.5 km and 31 km downstream distances, Figs 6a and 7a) but the relatively high C_v of this material means that the signal dies out rapidly downstream (Duller *et al.*, 2010). These bypass percentages are consistent with laboratory experiments on the interaction between axial and transverse channel systems (Kim *et al.*, 2011). Together the two fans therefore supply ~1.4 × 10^4 m^3 $year^{-1}$ of gravel to the axial river, which when combined with the supply coming from upstream (1.9 × 10^4 minus 5 × 10^3 = 1.4 × 10^4 m^3 $year^{-1}$; see *Grain size modelling - Axial Sperchios River*) give a total of ~2.8 × 10^4 m^3 $year^{-1}$, which is similar, within the uncertainty, to our estimate of gravel stored in the sub-basin to the Kobotades fault segment (i.e., 1.4 × 10^4–3.4 × 10^4 m^3 $year^{-1}$).

In summary, the grain size modelling indicates that ~1.1 × 10^4 m^3 $year^{-1}$ of coarse sediment is stored in the two large alluvial fans whereas 1.4 × 10^4–3.4 × 10^4 m^3 $year^{-1}$, is stored in stratigraphy along the axial fluvial system. We therefore obtain an estimate of the total volumetric gravel accumulation rate of 2.5 × 10^4–4.5 × 10^4 m^3 $year^{-1}$, or 2.5–4.5 × 10^8 m^3 for the Holocene (10 kyrs), for the transverse and axial fluvial systems combined, upstream of the delta plain. Note that this estimate is close to the lower estimate inferred from the geophysical data shown in Fig. 1b (i.e., 2.6 × 10^8–5.9 × 10^8 m^3) based on assuming a constant sedimentation rate. The agreement between these independent methods increases our confidence in this result.

Onshore erosional volumes

Modelling studies suggest that fault propagation and linkage within an active rift basin affect the location of the
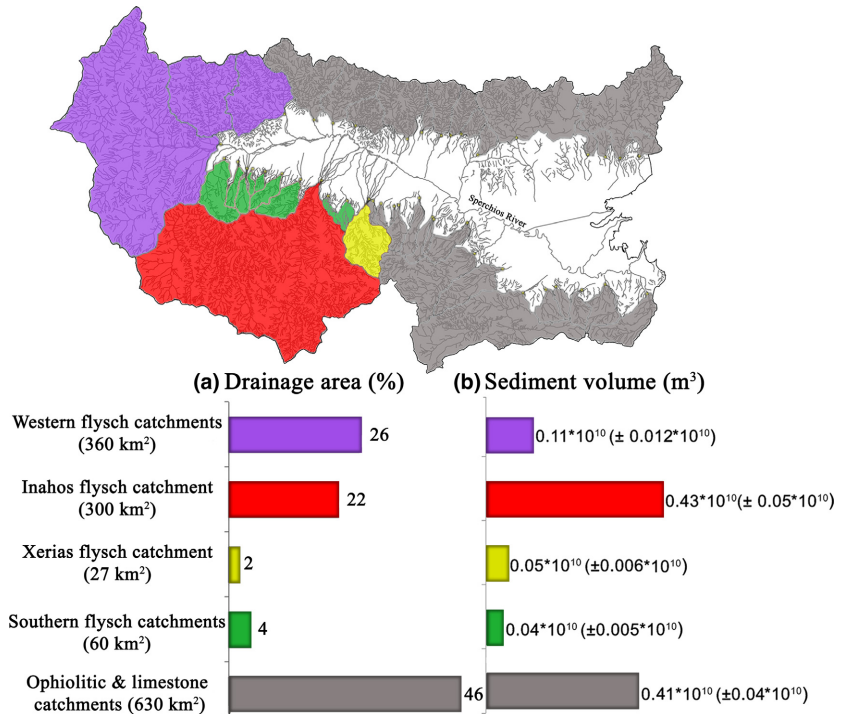
Fig. 9. (a) Bar chart showing the percentage of the total upstream drainage area of the main Sperchios catchments and (b) Bar chart showing sediment volumes (in m³) using average erosion rates (calibrated for the flysch catchments; see Methodology) and for the other catchments by assuming that the total volume of the 'closed system' is conserved.

main drainage divide and thus the volume of sediment supplied to a rift over time (Cowie *et al.*, 2006). Although we focus on a short time interval, i.e. the Holocene, we investigated this possibility by comparing the values of the transformed coordinate χ on opposite sides of the main Sperchios drainage divide for all the catchments that have a base-level at the coast, following the approach of Willett *et al.* (2014). Our analysis (see yellow arrows in Fig. 1 and Fig. S3) showed that >95% of the main drainage divide along the southern and western margins of the Sperchios rift appears to be stable as we did not observe any significant cross-divide contrasts in the χ values. Along the northern, hanging wall margin of the half graben, χ analysis could not be performed because the catchments lying to the north of the main drainage divide are internally drained and hence the base-level history is unconstrained. However, as this margin is tectonically relatively inactive the drainage divide is expected to be more stable. Thus, the total upland sediment source area has not changed significantly over the Holocene, i.e., the Sperchios River basin can be considered as a 'closed system'. Individual catchments along the tectonically active southern rift margin show evidence for local river diversion/capture (Eliet & Gawthorpe, 1995; see below) but sediment delivery remains directed towards the rift axis. Therefore, the overall mass balance for the source-to-sink system is unaffected (see *Summary and Discussion*).

A likely source material for the fine-grained Sperchios delta is the Paleogene flysch as it comprises interbedded layers of sandstones, friable siltstones and mudstone. It is one of the main lithologies particularly in the southwest

and western parts of the study area, exposed over 54% of the total upstream drainage area (Figs 1 and 9). The similar overall relief of the largest flysch catchments, plus their location near the rift tip, suggests that they are to some extent relict features of the pre-rift topography (Figs 1 and 9).

To quantify the volume of sediment released by erosion of the flysch during the Holocene we estimate catchment-average erosion rates by applying the modified stream-power erosion model (Eqn 2). We estimate the erodibility coefficient K using our field data of channel slope, S, and high flow channel width, W along the Inahos river (for location see Fig. 1a) and m = 0.6, n = 1.2 (see Eqns 1 and 2). We assume that river incision keeps pace with relative tectonic uplift where the river crosses the Kobotades fault and use a range of relative uplift rates of 0.5–0.75 mm year^{-1} (Whittaker & Walker, 2015). We thereby obtain values of K for the flysch that range between 1.5×10^{-6} and 2×10^{-6} m$^{-1/2}$ kg$^{-3/2}$ s^2. Similar values of the order of 10^{-5}–10^{-6} m$^{-1/2}$ kg$^{-3/2}$ s^2 have been inferred for settings composed of similar lithologies (e.g., Attal *et al.*, 2008).

Based on this calibration and applying Eqn (2) across the whole catchments area using every channel down to first order, we find that altogether the flysch catchments, which represent 54% of the total source area, account for 61% (~0.63 × 10^{10} m^3; Fig. 9b), of the total Holocene sediment supply. However, the Inahos catchment alone produces most (~68%) of all the sediment derived from the flysch, i.e., approximately 0.43 × 10^{10} ± 0.05 m^3 over the Holocene (Fig. 9b). Taking into account the

Western flysch catchment
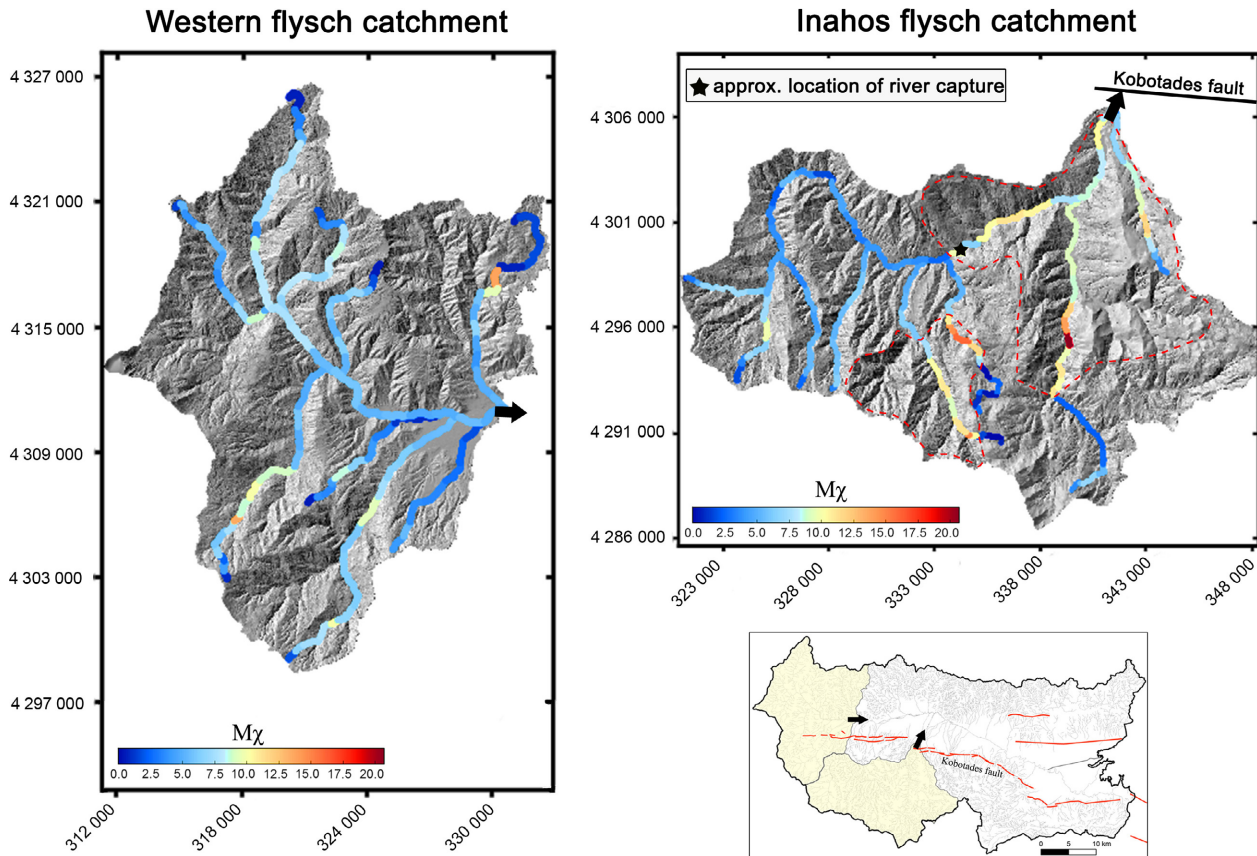

Inahos flysch catchment

Fig. 10. Map view of the channel slope in χ-elevation space ($M\chi$) on a hillshade for the western and the Inahos flysch catchments (see Methodology; Mudd *et al.*, 2014). The following values (defined in equation 1) were used: $m = 0.5$ and $n = 1$ that allowed a comparison for the two catchments. Cooler colors indicate lower values of $M\chi$ that imply lower erosion rates and warmer colors indicate higher values of $M\chi$ that imply higher erosion rates. Red dashed lines show areas of high stream power and steep hillslopes where erosion rates are >> 1 mm/yr across the Inahos flysch catchment (see also Fig. S4). Black thick arrows indicate the outlets of the two catchments. Inset shows the location map of the two catchments.

volume of sediment stored in the onshore fluvial systems ($2.5–4.5 \times 10^8$ m^3, see *Volume of sediment stored in the alluvial plain*), we can argue therefore that $\geq 40\%$ of the sediment that comprises the Sperchios delta (1×10^{10} m^3, see *Volume of sediment preserved in the delta*) is supplied by the Inahos catchment alone, even though it represents only 22% (Fig. 9a) of the source area of the entire Sperchios rift basin. Furthermore, these results imply an average erosion rate over this catchment (~1.5 mm year^{-1}) that exceeds the relative uplift rate at the fault and indicates that the catchment is not in steady state. A hillslope and curvature analysis of this catchment (Fig. S4) reveals its incised morphology. Steep hillslopes coupled to incising channels occur not only in the footwall of the active faults but also in upstream areas of this catchment and provide supporting evidence for high erosion rates (see dashed lines in Fig. 10 and Fig. S4). In contrast, the flysch catchments located at the western end of the Sperchios rift, cover a similar proportion of the total source area (i.e., ~26%; Fig. 9a) but release a much

smaller amount of sediment (~$0.11 \times 10^{10} \pm 0.012$ m^3) and account for only ~10% of the delta volume. The average erosion rate of this latter area is also lower, i.e., ~0.3 mm year^{-1}.

The contrast in implied erosion rates and sediment volumes for these two source areas within the flysch is revealed by maps of channel slope in χ-elevation space ($M\chi$) (Fig. 10). $M\chi$ is related to the ratio between erosion rate (E) and erodibility (K) (Mudd *et al.*, 2014) if the stream power law applies. Since both areas consist of the same bedrock lithology (i.e., $K \approx$ constant), higher $M\chi$ values imply higher erosion rates and vice versa. Differences in channel slope due to variations in bedload caliber can be excluded as the D$_{50}$ and D$_{84}$ are approximately the same for these two catchments (Riiser, 2016). The Inahos catchment is characterized by high erosion rates (warmer colours, Fig. 10), particularly in the eastern part, in a response to tectonic uplift in the proximal footwall of the Kobotades fault segment and in the zone of linkage with the Sperchias fault segment (Whittaker & Walker, 2015).
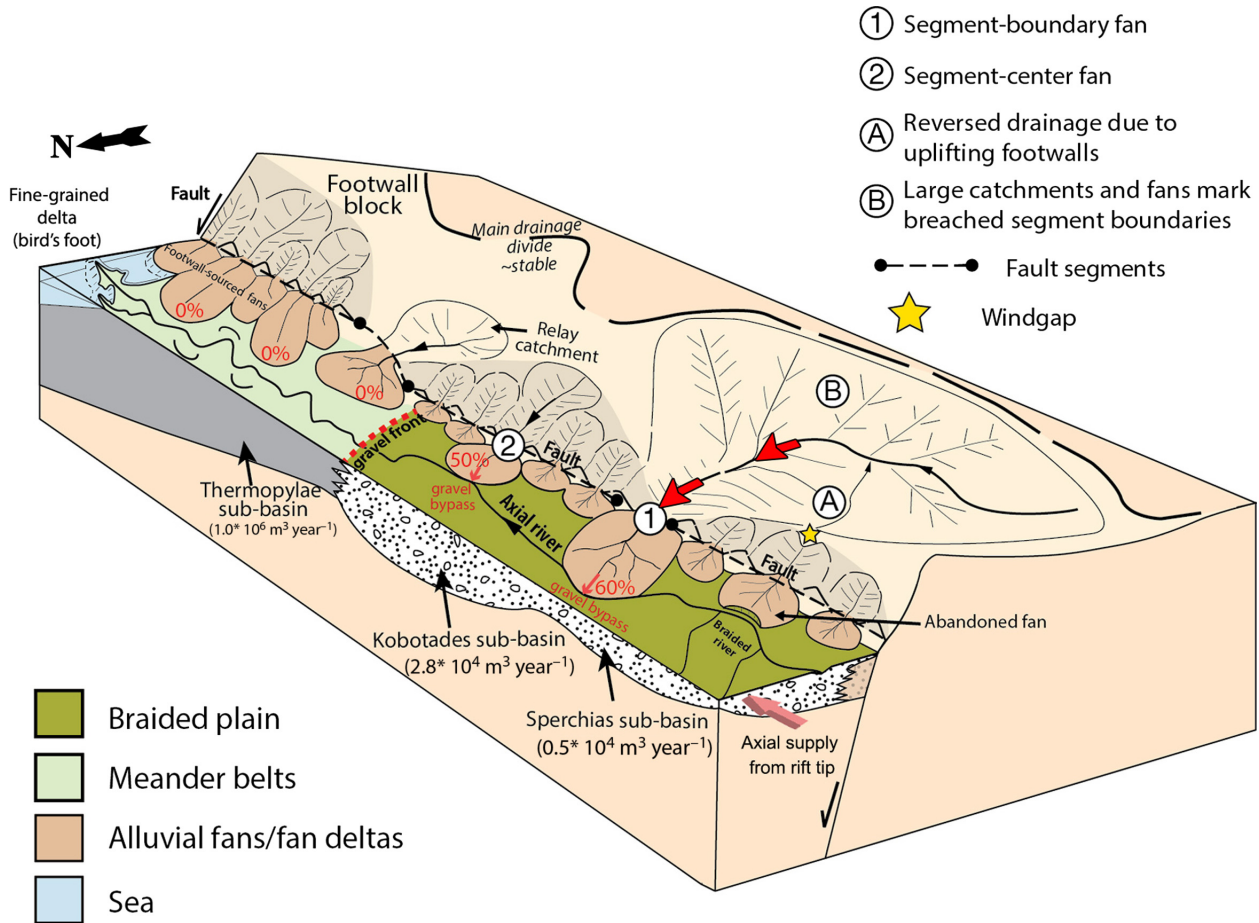
Fig. 11. Schematic summary of the Sperchios source-to-sink system. River capture events (see A) lead to the development of a large catchment (see B) at the footwall of active faults. Thick red arrows indicate high sediment supply from this catchment. Axial supply from the rift tip due to high relief pre-existing topography is shown with a thick pink arrow. Grain size fines down the axial river that passes from a braided to a meandering channel. The entire amount of the coarse fraction is extracted into stratigraphy leaving a fine-grained delta at the eastern part of the rift. The position of the gravel front is indicated with a red dashed line. Small red arrows show transverse gravel supply from fault segment–boundary and fault segment–center fans.

Note that erosion rates >1.5 mm year^{-1}, estimated using Eqn (2) and our estimate of K (red dashed lines, Fig. 10), occur in less than half of the Inahos catchment, which represents an even smaller fraction of the total source area. In contrast, the western flysch catchment depicts lower $M\chi$ and thus lower erosion rates (cooler colours, Fig. 10), consistent with this catchment lying at the tip of the rift beyond the zone of active normal faulting, thus not experiencing fault-controlled uplift.

The calculations above provide a first order constraint on the magnitude of the eroded volumes where the bedrock is flysch and allow variations to be highlighted between catchments that differ in terms of relative tectonic uplift rate. However, to estimate the volume of sediment supplied to the rift during the Holocene from the remaining catchments across the Sperchios River basin, where the bedrock lithology is not flysch, we first note

that the overall source-to-sink system has been a closed system at least over the Holocene (see Fig. S3). We then subtract the sediment volume supplied by all of the flysch catchments combined (~0.63 × 10^{10} m^3; Fig. 9a) from the total depositional volume preserved in the onshore fluvial systems and the Sperchios delta (1.025 × 10^{10} m^3– 1.045 × 10^{10} m^3). This calculation indicates that 0.41 × 10^{10} m^3, or 39%, of the total Holocene sediment supply, comes from the remaining (non–flysch) catchments (Fig. 9b), which cover 46% of the total source area. The bedrock in these catchments is comprised mainly of limestone (along the southern margin of the basin) and ophiolite (along the northern margin), which have lower erodibilities compared to the flysch. These lithologies are seen preserved in coarse-grained alluvial fans along the rift margins but are only sparsely represented (by coarse sands and occasional pebbles within channel fills) in the

Holocene deltaic deposits (Pechlivanidou *et al.*, 2014). Therefore, even though the Thermopylae segment is bounded along its south side by active normal faults, the limestones catchments in this area are not the dominant source of the axial fill within the rift because most of the eroded material is trapped along the basin margin (Fig. 3). This is confirmed by the borehole samples described in Pechlivanidou *et al.*, 2014 (see Fig. 3a for location of boreholes).

SUMMARY AND DISCUSSION

A schematic summary of our results for the Sperchios source-to-sink system is presented in Fig. 11. The Sedflux2D modelling indicated that a total sediment supply of 1×10^6 m^3 year^{-1}, of predominantly sand and silt, is needed to build the Sperchios bird's foot delta within a period of 10 000 years. We validated this estimate by comparing model output with the observed stratigraphic architecture of the delta and independent constraints on its total thickness. By using Sedflux2D we obtained better constraints on both sub-aerial and submarine sedimentation and were also able to take into account both eustatic and tectonic accommodation creation along the Thermopylae segment of the rift. The main limitation in the Sedflux2D modelling is our assumption of a constant rate in sediment supply throughout the simulation time (10 000 years). High-frequency climatic shifts during the Holocene (Zanchetta *et al.*, 2011; Gogou *et al.*, 2016) probably affected the rates of sediment delivery but in this study we are concerned with the Holocene-averaged supply and not the variability in supply due to climatic forcing.

Using 'χ analysis' we demonstrated the stability of the main drainage divide at least along the most active, southern, rift margin and thus we are able to demonstrate that long term changes in the total sediment supply are unlikely to have significantly affected the Holocene depositional history, i.e., the Sperchios rift basin is a 'closed' system. The boundaries of individual catchments along the southern rift margin do show evidence for being unstable, consistent with the active tectonic setting (e.g., Cowie *et al.*, 2006), and there is field evidence for local river capture (e.g., Eliet & Gawthorpe, 1995; Fig. 10). Although individual catchments probably have supplied a variable amount of sediment over time, the timescale of this variation is set by the landscape response to fault growth and particularly segment linkage, which is thought to have occurred ~1.6 Ma (Whittaker & Walker, 2015) and therefore does not influence significantly the sediment supply during the Holocene. Furthermore, we are concerned here with the overall sediment budget for the entire source-to-sink system, not the fluctuations in the volume of sediment derived from specific catchments

that might arise due to river capture. In summary, therefore, the overall source-to-sink system of the Sperchios rift has remained a 'closed system' over the timescale of the Holocene.

Our grain size modelling of the alluvial fans and braided axial river indicates that a linear increase in the rate of hanging wall accommodation creation from west to east along the rift axis and a total gravel supply of 2.5×10^4–4.5×10^4 m^3 year^{-1} can explain the observed downstream grain size fining trend and the present-day position of the gravel front near the eastern tip of the Kobotades fault segment. Where the gravel is eventually exhausted there is an associated downstream change in the fluvial morphology from a braided to a meandering channel and mainly sand and silt only are ultimately transported to the delta. Changes in tectonic subsidence rate through time along the rift could lead to variations in the position of the gravel front, e.g., if more (or less) of the coarse material is extracted in to stratigraphy at the rift tip. Our grain size measurements only reflect characteristics of the modern river and there is uncertainty about the active fluvial valley width. However, our volume estimates compared well with those inferred from gravity data (Fig. 1b) and estimates of the age of the rift. In fact, Whittaker & Walker's (2015) preferred tectonic model for the evolution of the Sperchios rift (extension initiated ~3.6 Ma and rates of fault slip increased by a factor of ×3 at ~1.6 Ma) would imply a volumetric sedimentation rate since ~1.6 Ma of 4.2×10^4 m^3 year^{-1} for the Sperchias and Kobotades segments combined, which is very close to our upper estimate. This not only lends confidence to our results but also suggests that the pattern of tectonic subsidence, at least along this part of the rift, has remained relatively stable over long time periods.

Our grain size analysis of the two main footwall-sourced alluvial fan systems suggests, in addition, that location of fluvial systems relative to fault segmentation, and the associated variations in relative tectonic uplift/subsidence, influence gravel delivery to hanging wall depositional systems. We found that the catchment that feeds the Inahos fan, through the zone of linkage between the Kobotades and Sperchias fault segments, produces approximately double the amount of gravel compared to the Xerias catchment, located near the centre of the Kobotades fault segment, due to its much larger drainage area (i.e., Q_{so} ~1.7×10^4 m^3 year^{-1} for Inahos and Q_{so} ~0.8×10^4 m^3 year^{-1} for Xerias; see Fig. 8a,b). However, the Xerias catchment produces coarser material and a higher gravel fraction due to its location in an area of higher uplift rates near the central part of the fault segment, i.e., for Xerias $D_{50} = 81.5$ mm and the gravel fraction is ~16% whereas for Inahos, $D_{50} = 52$ mm and gravel represents ~4%. The overall gravel fraction of the entire Holocene depositional system is estimated to be 3–5% of the total sediment
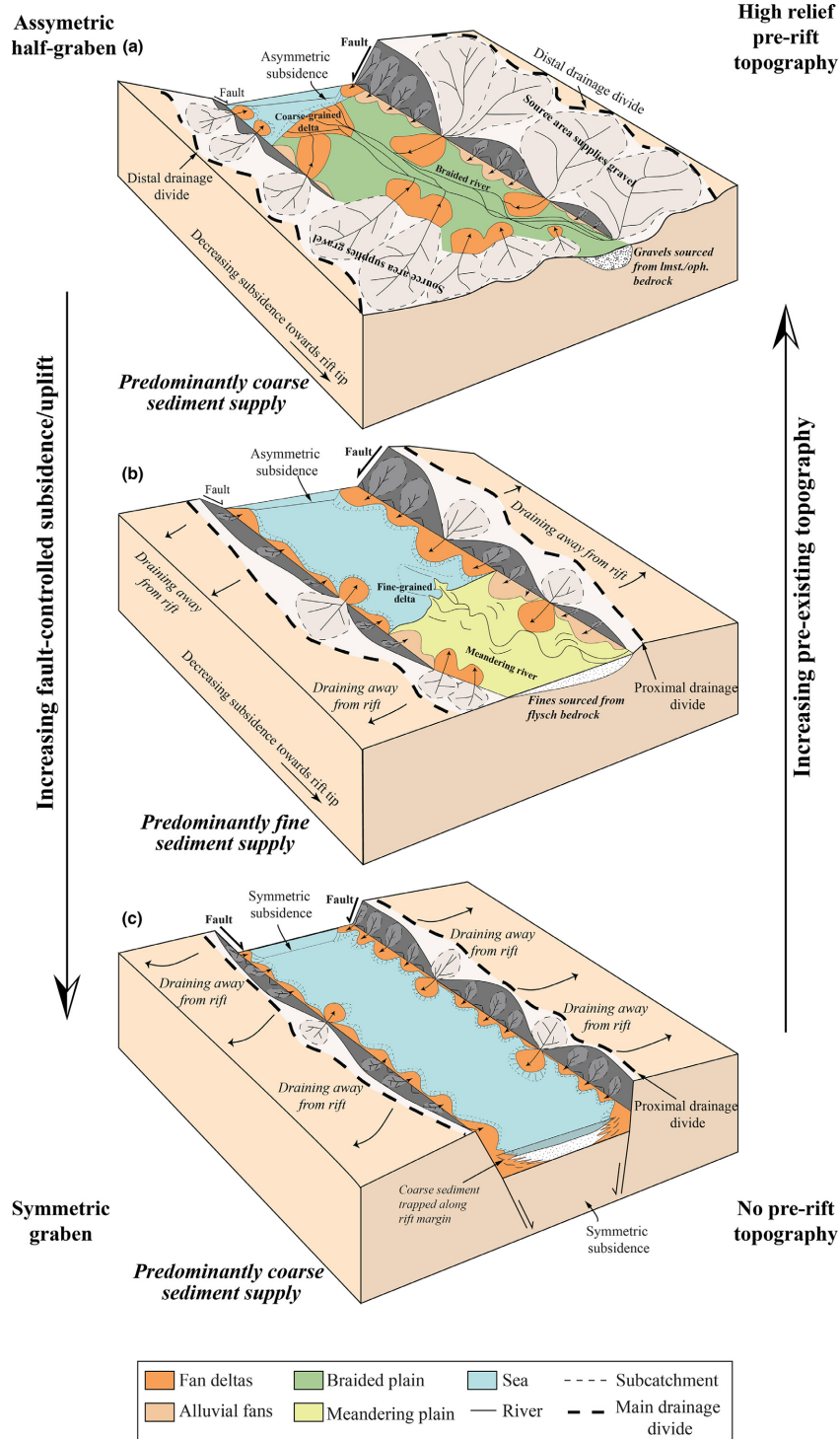
Fig. 12. Schematic block diagrams of three rift settings (a), (b) and (c) to illustrate the impact of sediment supply characteristics and rate of accommodation creation on depositional architectures within rift basins. Fault-controlled subsidence along rift margins increases from (a) to (c). Pre-existing topography increases from (c) to (a). Coarse-grained sources characterize (a) and (c) and fine-grained sources characterize (b). Note the change of the location of the main drainage divide from distal in (a) to proximal in (c). In rift setting shown in (a), the sediment routing system is characterized by an axially flowing braided river that interacts with transverse fans emerging from the tips of fault segments and forms a coarse-grained delta. In rift setting shown in (b), the axial river forms meandering belts and a fine-grained delta. Alluvial fans and fan deltas prograde into the basin and interact with the axial river. In (c), the rift is characterized by a marine basin. Footwall-sourced fan deltas are building aggradational units close to the border fault zones at both rift margins.

supply. However, this is a minimum estimate because abrasion may have also contributed to reducing grain size and, furthermore, there are other alluvial fans in the Sperchios basin that do not feed the delta (Fig. 1a). This estimate of the gravel fraction is consistent with previous work (Syvitski, 2011) but our study demonstrates that there is a strong spatial variation in gravel inputs into the source-to-sink system.

Many source-to-sink studies use empirically-derived models such as the 'BQART' model of Syvitski & Milliman (2007) to predict sediment supply rates and thus calculate sediment budgets for depositional systems (e.g., Sømme *et al.*, 2011). However, the 'BQART' model does not capture the potentially large variations in surface processes and rates that characterize landscapes in tectonically settings such as the Sperchios rift. For example, the 'BQART' model would predict similar sediment production from the Inahos and the western flysch catchments, as both are characterized by similar drainage areas, maximum relief, lithology and climatic conditions. In contrast, our analysis suggests that they differ in terms of sediment production by about a factor of ×4 (Fig. 9b). Our calculations reveal that nearly 70% of the sediment supply derived from all the flysch catchments combined comes from the Inahos catchment, which represents less than half the area where flysch is exposed. This catchment, located in the mutual footwall of the Kobotades and Sperchias fault segments (see B on Fig. 11), exhibits the highest erosion rates in a relatively small part of this catchment located in the proximal footwall to the Kobotades fault. This catchment experienced a doubling of its drainage area when the main channel captured the upper reaches of the catchments draining the footwall of the Sperchias fault segment (see star on Fig. 11). The capture event is well-documented by an abandoned alluvial fan (Fig. 11), emerging from the footwall along Sperchias fault segment, for which the source area is no longer evident (Eliet & Gawthorpe, 1995). The cause of the capture is most likely related to fault segment linkage that occurred ~1.6 Ma (Whittaker & Walker, 2015) and led to a change in the pattern of footwall uplift. Thus, we can attribute the high sediment flux from Inahos catchment to a transient landscape response, over a timescale of 1–2 million years, in response to an increase in relative tectonic uplift in the linkage area as well as an increase in drainage area. In contrast, the sediment supply from the western catchments is a consequence of the pre-existing (i.e., pre-extension) topography beyond the rift tip as tectonic uplift rates in this area are low.

Finally, by combining the evidence that the Sperchios rift has been a 'closed' source-to-sink system over the Holocene, with our estimates for the sediment supply from all of the flysch catchments, and the total depositional volume in the fluvial-deltaic system, we are able to show that ≥ 40% of the sediment that builds the Sperchios delta is supplied by the Inahos catchment alone even though it represents ≤22% of the entire source area. The fine grained character of the delta is thus due to the combination of (1) the dominant source area being in the flysch plus (2) the trapping of coarse material within transverse alluvial fans and (3) deposition of gravel bars and other channel sediments along the axial river within the Sperchias and Kobotades segments of the rift.

Implications

This study allows us to identify and assess the relative importance of key controls in the development of the Sperchios rift source-to-sink system: (1) the role of pre-existing topography in influencing the location of the main drainage divide in the area of the rift tip, (2) bedrock lithology and its influence on the grain size of source material delivered to the rift, and (3) lateral variations in the rate of tectonic uplift/subsidence that control patterns of erosion and deposition. By generalizing these results, we can predict the response of the shoreline and the gravel front to the volume and characteristics of supplied sediment and to accommodation creation, thus improving our broader understanding of sequence evolution in extensional settings.

Figure 12 shows three schematic block diagrams of rift settings, based on generalizations of the Sperchios rift itself, where tectonic accommodation creation increases (left-hand axis; from top to bottom). We also allow for a variation from the case of an asymmetric half-graben to the case of a symmetric graben. At the same time, the relief of the pre-rift topography increases (right-hand axis; from bottom to top), which has the effect of shifting the main drainage divide from a location in the proximal footwall of the rift-bounding faults to a more distal position as a result of a relatively mountainous landscape that existed prior to the initiation of extension. Furthermore, we allow for variations in source lithology (e.g., limestone, ophiolite, Fig. 12a,c vs. flysch, Fig. 12b) that determine the relative amounts of coarser vs. finer sediment supply to the rift.

In the case where the rift is characterized by low rates of accommodation creation and high palaeotopography (Fig. 12a), so that the main drainage divide is at a distal location, large volumes of sediment are supplied to the rift tip. In this scenario, and assuming that the source area supplies relatively coarse grained material, extensive alluvial fans and a braided channel domain will be developed and a coarse-grain delta will form at the shoreline. In the second case scenario (Fig. 12b), the main drainage divide is at a more proximal position, controlled by footwall uplift along the rift-bounding normal faults, and hence less sediment is supplied to the rift tip. In

this scenario, if we further assume that the source area is dominated by flysch and that the coarse sediment fraction is trapped entirely in hanging wall alluvial fans close to the rift margins (Fig. 12b), then a more extensive meandering axial fluvial channel forms and a fine-grained delta develops where it debouches into the sea. However, the reduced volume of the sediment supply means that the delta forms closer to the rift tip compared to the present-day position of the Sperchios delta. In the third case scenario (Fig. 12c), subsidence occurs along both rift margins (i.e., a symmetric rift) as well as the total sediment supply being limited by the proximal position of the main drainage divide. Coarse sediment, derived from steep catchments draining the scarps of the basin bounding faults is mainly trapped along the rift margins in transverse fan-deltas and subsidence exceeds sediment supply overall. These conditions favour the development of an underfilled open marine or lacustrine basin.

CONCLUSIONS

The aim of this study has been to understand controls on sediment supply, transport and deposition within an active rift setting from a source-to-sink perspective. Via our analysis of the Sperchios rift basin, in central Greece, we demonstrate explicitly how characteristics of the sediment supply, the rate of accommodation creation and pre-rift topography, control depositional patterns and facies development. We show the importance of integrating different data types and modelling approaches with field observations in order to understand how complex source-to-sink systems function. Specifically, we use a numerical model to quantify sedimentation rates in an area where accommodation creation is controlled by both sea-level variations and tectonics, grain size analysis to quantify spatial variations in gravel production and storage along the transport system, the stream power model to estimate average erosion rates, and 'χ analysis' to reveal spatial variations in erosion rates as well as to investigate the stability of drainage divides. Combining all of this information allows us to calculate the sediment budget for the offshore and onshore depositional system and to perform a mass-balance analysis for the Sperchios rift over the Holocene.

We demonstrate that the Sperchios rift comprises a 'closed' system at least over the Holocene, so that the sum of the sediment volumes deposited at the delta ($\sim 1 \times 10^{10}$ m³) and along the routing system ($\sim 4 \times 10^{8}$ m³) during the Holocene balances the sediment volumes released from the upland source areas. Tectonic subsidence modulates the characteristics of the sediment supply leading to a significant grain size fining along the axial system. All the coarse material is extracted into the stratigraphy due to selective deposition, resulting in the formation of an extensive meandering belt (>15 km) that feeds the fine-grained Sperchios delta. Approximately half of the coarse supply is produced from transverse catchments that cross the border fault zone, controlling the south margin of the Sperchios rift. Abrasion is not required to explain the grain size fining trends. Moreover, we show that one catchment in particular (Inahos) covers only 22% of the Sperchios upland drainage area but releases >40% of the total sediment that builds the Holocene delta. High erodibility of the bedrock lithology (Paleogene flysch), active normal faulting and a long-term transient landscape response to fault segment linkage, together can explain the higher sediment supply from this catchment. The flysch is the source of the relatively large volume of silt and sand that produces the characteristic bird's foot geometry of the Sperchios delta.

Finally, the quantitative process based models used in this study provide a greater understanding of the source-to-sink system because they not only allow quantitative characterization of source areas but also link accommodation creation and depositional volumes with grain size variation and facies development.

SUPPORTING INFORMATION

Additional Supporting Information may be found in the online version of this article:

Figure S1. (a) Coefficient of variation, *Cv*, against downstream distance along the Sperchios River calculated for grains size distributions measured for active gravel bars. (b) and (c) Same as in (a) but for the two large alluvial fans.
Figure S2. Plot showing the predicted grain size distributions due to different spatial variations in basin subsidence rate (a, b) and (c) mass loss from the abrasion process compared with the measured grain size data along

the axial system (black dots).

Figure S3. Map view of chi (χ) values calculated on the opposite sides of the main Sperchios drainage divide for all catchments with a base-level at the coast, following the approach of Willett *et al.* (2014) and using m/n = 0.5.

Figure S4. Slope map of the Inahos flysch catchment with all slopes <25° shown with grey colour and slopes >25° shown with orange to red colours.

REFERENCES

ALLEN, P.A. (2008) From landscapes into geological history. *Nature*, **451**, 274–276.

ALLEN, P.A. & DENSMORE, A.L. (2000) Sediment flux from an uplifting fault block. *Basin Res.*, **12**, 367–380.

ALLEN, P.A., ARMITAGE, J.J., CARTER, A., DULLER, R.A., MICHAEL, N.A., SINCLAIR, H.D., WHITCHURCH, A.L., WHITTAKER, A.C. & SCHLUNEGGER, F. (2013) Theqsproblem: sediment volumetric balance of proximal foreland basin systems. *Sedimentology*, **60**, 102–130.

ALLEN, P.A., ARMITAGE, J.J., WHITTAKER, A.C., MICHAEL, N.A., RODA-BOLUDA, D. & D'ARCY, M. (2015) Fragmentation model of the grain size mix of sediment supplied to basins. *J. Geol.*, **123**, 405–427.

APOSTOLOPOULOS, G. (2005) Geophysical studies relating to the tectonic structure, geothermal fields and geomorphological evolution of the Sperchios River Valley, Central Greece. *J. Balkan Geophys. Soc.*, **8**, 99–112.

ARMIJO, R., MEYER, B., KING, G.C.P., RIGO, A. & PAPANASTASSIOU, D. (1996) Quaternary evolution of the Corinth rift and its implications for the late Cenozoic evolution of the Aegean. *Geophys. J. Int.*, **126**, 11–53.

ARMITAGE, J.J., DULLER, R.A., WHITTAKER, A.C. & ALLEN, P.A. (2011) Transformation of tectonic and climatic signals from source to sedimentary archive. *Nat. Geosci.*, **4**, 231–235.

ARMITAGE, J.J., ALLEN, P.A., BURGESS, P.M., HAMPSON, G.J., WHITTAKER, A.C., DULLER, R.A. & MICHAEL, N.A. (2015) Sediment transport model for the Eocene Escamilla sediment-routing system: implications for the uniqueness of sequence stratigraphic architectures. *J. Sediment. Res.*, **85**, 1510–1524.

ATTAL, M. & LAVÉ, J. (2006) Changes of bedload characteristics along the Marsyandi River (Central Nepal): implications for understanding hillslope sediment supply, sediment load evolution along fluvial networks, and denudation in active Orogenic belts. *GSA Spec. Paper.*, **398**, 143–171.

ATTAL, M. & LAVÉ, J. (2009) Pebble abrasion during fluvial transport: experimental results and implications for the evolution of the sediment load along rivers. *J. Geophys. Res.*, **114**, F0402.

ATTAL, M., TUCKER, G.E., WHITTAKER, A.C., COWIE, P.A. & ROBERTS, G.P. (2008) Modeling fluvial incision and transient landscape evolution: influence of dynamic channel adjustment. *J. Geophys. Res.*, **113**, F03013.

ATTAL, M., COWIE, P.A., WHITTAKER, A.C., HOBLEY, D., TUCKER, G.E. & ROBERTS, G.P. (2011) Testing fluvial erosion models using the transient response of Bedrock Rivers to tectonic forcing in the Apennines, Italy. *J. Geophys. Res.*, **116**, F02005.

COVAULT, J.A., ROMANS, B.W., FILDANI, A., MCGANN, M. & GRAHAM, S.A. (2010) Rapid climatic signal propagation from source to sink in a Southern California sediment routing system. *J. Geol.*, **118**, 247–259.

COVAULT, J.A., ROMANS, B.W., GRAHAM, S.A., FILDANI, A. & HILLEY, G.E. (2011) Terrestrial source to deep-sea sink sediment budgets at high and low sea levels: insights from tectonically active Southern California. *Geology*, **39**, 619–622.

COWIE, P.A. & SHIPTON, Z.K. (1998) Fault tip displacement gradients and process zone dimensions. *J. Struct. Geol.*, **20**, 983–997.

COWIE, P.A., ATTAL, M., TUCKER, G.E., WHITTAKER, A.C., NAYLOR, M., GANAS, A. & ROBERTS, G.P. (2006) Investigating the surface process response to fault interaction and linkage using a numerical modelling approach. *Basin Res.*, **18**, 231–266.

COWIE, P.A., WHITTAKER, A.C., ATTAL, M., ROBERTS, G., TUCKER, G.E. & GANAS, A. (2008) New constraints on sediment-flux–dependent river incision: implications for extracting tectonic signals from river profiles. *Geology*, **36**, 535.

D'ARCY, M., WHITTAKER, A.C., RODA-BOLUDA, D.C. & BRISTOW, C. (2016) Measuring alluvial fan sensitivity to past climate changes using a self-similarity approach to grain size fining, Death Valley, California. *Sedimentology*, **64**, 388–424.

DENSMORE, A.L., ALLEN, P.A. & SIMPSON, G. (2007) Development and response of a coupled catchment fan system under changing tectonic and climatic forcing. *J. Geophys. Res.*, **112**, F01002, https://doi.org/10.1029/2006JF000474.

DULLER, R.A., WHITTAKER, A.C., FEDELE, J.J., WHITCHURCH, A.L., SPRINGETT, J., SMITHELLS, R., FORDYCE, S. & ALLEN, P.A. (2010) From grain size to tectonics. *J. Geophys. Res.*, **115**, F03022, https://doi.org/10.1029/2009JF001495.

ELIET, P.P. (1995) Geomorphology and Tectono-Sedimentary Interactions within Active Rift Environments: The Sperchios Basin, Central Greece, University of Manchester.

ELIET, P.P. & GAWTHORPE, R.L. (1995) Drainage development and sediment supply within rifts, examples from the Sperchios Basin, Central Greece. *J. Geol. Soc.*, **152**, 883–893.

FEDELE, J.J. & PAOLA, C. (2007) Similarity solutions for fluvial sediment fining by selective deposition. *J. Geophys. Res.*, **112**, F02038, https://doi.org/10.1029/2005JF000409 .

FINNEGAN, N.J., ROE, G., MONTGOMERY, D.R. & HALLET, B. (2005) Controls on the channel width of rivers: implications for modeling fluvial incision of bedrock. *Geology*, **33**, 229.

FORZONI, A., STORMS, J.E.A., WHITTAKER, A.C. & DE JAGER, G. (2014) Delayed delivery from the sediment factory: modeling the impact of catchment response time to tectonics on sediment flux and fluvio-deltaic stratigraphy. *Earth Surf. Proc. Land.*, **39**, 689–704.

GOGOU, A., TRIANTAPHYLLOU, M., XOPLAKI, E., IZDEBSKI, A., PARINOS, C., DIMIZA, M., BOULOUBASSI, I., LUTERBACHER, J., KOULI, K., MARTRAT, B., TORETI, A., FLEITMANN, D., ROUSAKIS, G., KABERI, H., ATHANASIOU, M. & LYKOUSIS, V. (2016) Climate variability and socio-environmental changes in the Northern Aegean (Ne Mediterranean) during the last 1500 years. *Quatern. Sci. Rev.*, **136**, 209–228.

GOLDSWORTHY, M., JACKSON, J. & HAINES, J. (2002) The continuity of active fault systems in Greece. *Geophys. J. Int.*, **148**, 596–618.

HAMPSON, G.J., DULLER, R.A., PETTER, A.L., ROBINSON, R.A.J. & ALLEN, P.A. (2014) Mass-balance constraints on stratigraphic interpretation of linked alluvial-coastal-shelfal deposits from source to sink: example from Cretaceous Western Interior Basin, Utah and Colorado, U.S.A. *J. Sediment. Res.*, **84**, 935–960.

HELLER, P. & PAOLA, C. (1992) The large-scale dynamics of grain size variation in alluvial basins, 2: application to syntectonic conglomerate. *Basin Res.*, **4**, 91–102.

HUTTON, E.W.H. & SYVITSKI, J.P.M. (2008) Sedflux 2.0: an advanced process-response model that generates three-dimensional stratigraphy. *Comput. Geosci.*, **34**, 1319–1337.

JORDAN, T.E. & FLEMINGS, P.B. (1991) Large-scale stratigraphic architecture, eustatic variation, and unsteady tectonism: a theoretical evaluation. *J. Geophys. Res. Solid Earth*, **96**, 6681–6699.

KILIAS, A.A., TRANOS, M.D., PAPADIMITRIOU, E.E. & KARAKOSTAS, V.G. (2008) The recent crustal deformation of the Hellenic Orogen in Central Greece; the Kremasta and Sperchios fault systems and their relationship with the adjacent large structural features. *Zeitschrift der Deutschen Gesellschaft für Geowissenschaften – German Journal of Geology (ZDGG)*, **159**, 533–547.

KIM, W., CONNELL, S.D., STEEL, E., SMITH, G.A. & PAOLA, C. (2011) Mass-balance control on the interaction of axial and transverse channel systems. *Geology*, **39**, 611–614.

LAMBECK, K. & PURCELL, A. (2005) Sea-level change in the mediterranean sea since the Lgm: model predictions for tectonically stable areas. *Quatern. Sci. Rev.*, **24**, 1969–1988.

LEEDER, M.R. & JACKSON, J.A. (1993) The interaction between normal faulting and drainage in active extensional basins, with examples from the Western United States and Central Greece. *Basin Res.*, **5**, 79–102.

MATENCO, L. & ANDRIESSEN, P. (2013) Quantifying the mass transfer from mountain ranges to deposition in sedimentary basins: source to sink studies in the Danube Basin–Black Sea System. *Global Planet. Change*, **103**, 1–18.

MICHAEL, N.A., WHITTAKER, A.C. & ALLEN, P.A. (2013) The functioning of sediment routing systems using a mass balance approach: example from the Eocene of the Southern Pyrenees. *J. Geol.*, **121**, 581–606.

MICHAEL, N.A., WHITTAKER, A.C., CARTER, A. & ALLEN, P.A. (2014) Volumetric budget and grain size fractionation of a geological sediment routing system: Eocene Escanilla formation, South-Central Pyrenees. *Geol. Soc. Am. Bull.*, **126**, 585–599.

MUDD, S.M., ATTAL, M., MILODOWSKI, D.T., GRIEVE, S.W.D. & VALTERS, D.A. (2014) A statistical framework to quantify spatial variation in channel gradients using the integral method of channel profile analysis. *J. Geophys. Res., series F*, **119**, 138–152.

ORTON, G.J. & READING, H.G. (1993) Variability of deltaic processes in terms of sediment supply, with particular emphasis on grain size. *Sedimentology*, **40**, 475–512.

PAOLA, C. (2000) Quantitative models of sedimentary basin filling. *Sedimentology*, **47**, 121–178.

PAOLA, C., HELLER, P. & ANGEVINE, C. (1992) The large-scale dynamics of grain size variation in alluvial basins: 1. Theory. *Basin Res.*, **4**, 73–90.

PECHLIVANIDOU, S. (2012) Modeling the sedimentological and the geomorphological evolution of the Sperchios deltaic sequence during Holocene. *Doctoral Thesis*, Aristotle University of Thessaloniki, 229 pp (in Greek; English abstract).

PECHLIVANIDOU, S., VOUVALIDIS, K., LOVLIE, R., NESJE, A., ALBANAKIS, K., PENNOS, C., SYRIDES, G., COWIE, P. & GAWTHORPE, R. (2014) A multi-proxy approach to reconstructing sedimentary environments from the Sperchios Delta, Greece. *Holocene*, **24**, 1825–1839.

PERRON, J.T. & ROYDEN, L. (2013) An integral approach to bedrock river profile analysis. *Earth Surf. Proc. Land.*, **38**, 570–576.

POULOS, S., LEONTARIS, S. & COLLINS, M.B. (1997) Sedimentological and clay mineralogical investigations in Malliakos Gulf, Eastern Greece. *Bollet. Geofis. Teorit. Appl.*, **38**, 267–279.

RIISER, O.S. (2016) Using grain size analysis to understand transverse versus axial sediment supply to a rift: Example from the Sperchios rift, Greece. Master Thesis, University of Bergen.

ROHAIS, S., BONNET, S. & ESCHARD, R. (2012) Sedimentary record of tectonic and climatic erosional perturbations in an experimental coupled catchment-fan system. *Basin Res.*, **24**, 198–212.

ROYDEN, L. & PERRON, J.T. (2013) Solutions of the stream power equation and application to the evolution of river longitudinal profiles. *J. Geophys. Res. Earth Surf.*, **118**, 497–518.

SØMME, T.O., HELLAND-HANSEN, W., MARTINSEN, O.J. & THURMOND, J.B. (2009) Relationships between morphological and sedimentological parameters in source-to-sink systems: a basis for predicting semi-quantitative characteristics in subsurface systems. *Basin Res.*, **21**, 361–387.

SØMME, T.O., PIPER, D.J.W., DEPTUCK, M.E. & HELLAND-HANSEN, W. (2011) Linking onshore-offshore sediment dispersal in the golo source-to-sink system (Corsica, France) during the late quaternary. *J. Sediment. Res.*, **81**, 118–137.

SØMME, T.O., MARTINSEN, O.J. & LUNT, I. (2013) Linking offshore stratigraphy to onshore paleotopography: the late Jurassic-Paleocene evolution of the South Norwegian margin. *Geol. Soc. Am. Bull.*, **125**, 1164–1186.

SYVITSKI, J.P.M. (2011) Global sediment fluxes to the earth's coastal ocean. *Appl. Geochem.*, **26**, S373–S374.

SYVITSKI, J.P.M. & HUTTON, E.W.H. (2001) 2d Sedflux 1.0c. *Comput. Geosci.*, **27**, 731–753.

SYVITSKI, J.P.M. & MILLIMAN, J.D. (2007) Geology, geography, and humans battle for dominance over the delivery of fluvial sediment to the coastal ocean. *J. Geol.*, **115**, 1–19.

VISHER, G.S. (1969) Grain size distributions and depositional processes. *J. Sediment. Petrol.*, **39**, 1074–1106.

WHIPPLE, K.X. & TUCKER, G.E. (1999) Dynamics of the stream-power river incision model: implications for height limits of mountain ranges, landscape response timescales, and research need. *J. Geophys. Res.*, **104**, 17661–17674.

WHITTAKER, A.C. & WALKER, A.S. (2015) Geomorphic constraints on fault throw rates and linkage times: examples from the Northern Gulf of Evia, Greece. *J. Geophys. Res., series F*, **120**, 137–158.

WHITTAKER, A.C., COWIE, P.A., ATTAL, M., TUCKER, G.E. & ROBERTS, G.P. (2007) Bedrock channel adjustment to tectonic forcing: implications for predicting river incision rates. *Geology*, **35**, 103.

WHITTAKER, A.C., ATTAL, M. & ALLENN, P.A. (2010) Characterising the origin, nature and fate of sediment exported from catchments perturbed by active tectonics. *Basin Res.*, **22**, 809–828.

WHITTAKER, A.C., DULLER, R.A., SPRINGETT, J., SMITHELLS, R.A., WHITCHURCH, A.L. & ALLEN, P.A. (2011) Decoding downstream trends in stratigraphic grain size as a function of tectonic subsidence and sediment supply. *Geol. Soc. Am. Bull.*, **123**, 1363–1382.

WILLETT, S.D., MCCOY, S.W., PERRON, J.T., GOREN, L. & CHEN, C.Y. (2014) Dynamic reorganization of river basins. *Science*, **343**, 1248765.

ZANCHETTA, G., SULPIZIO, R., ROBERTS, N., CIONI, R., EASTWOOD, W.J., SIANI, G., CARON, B., PATERNE, M. & SANTACROCE, R. (2011) Tephrostratigraphy, chronology and climatic events of the Mediterranean basin during the Holocene: an overview. *Holocene*, **21**, 33–52.